WHY OLD PULSARS DO NOT GLITCH OFTEN

By

Kuba Girma

SUBMITTED IN PARTIAL FULFILLMENT OF THE
REQUIREMENTS FOR THE DEGREE OF
MASTER OF SCIENCE IN PHYSICS
AT
ADDIS ABABA UNIVERSITY
ADDIS ABABA, ETHIOPIA
JUNE 2014

ADDIS ABABA UNIVERSITY
COLLEGE OF NATURAL SCIENCES
FACULTY OF CHEMICAL AND PHYSICAL SCIENCE
DEPARTMENT OF PHYSICS

The undersigned hereby certify that they have read and recommend to the School of Graduate Studies for acceptance a thesis entitled "**Why Old Pulsars Do Not Glitch Often** " by **Kuba Girma** in partial fulfillment of the requirements for the degree of **Master of Science in Physics**.

Dated: June 2014

Supervisor: _____
Dr. Legese Wetro

Examiners: _____
Prof. A. K. Chaubay

_____
Prof. A. V. Gholap

ADDIS ABABA UNIVERSITY

Date: **June 2014**

Author: **Kuba Girma**

Title: **Why Old Pulsars Do Not Glitch Often**

Department: **Physics**

Degree: **M.Sc.** Convocation: **June** Year: **2014**

Permission is herewith granted to Addis Ababa University to circulate and to have copied for non-commercial purposes, at its discretion, the above title upon the request of individuals or institutions.

Signature of Author

To my uncle Tesfaye Abebe

Table of Contents

List of Figures

Abstract

Some pulsars are stable in the universe, even though, many of them glitch i.e. their spin frequencies increase suddenly. Young pulsars, such as the crab pulsar glitch within short period of time i.e. they glitch within a few years. However, old pulsars do not glitch as such. This thesis tries to analyze the causes behind these glitches and why their frequencies decrease with the ages of pulsars. We study the gravitational tidal force interaction between the core and the crust and employs its effect on the long term evolution of pulsar glitches. In particular, we have shown that old pulsars show less glitches proportional to their ages and also we derived the time at which the crust and the core of neutron star will be tidally locked.

Key Words: star: neutron star, pulsars: general, glitch: pulsar , tidal interaction.

Acknowledgements

First of all, I would like to thank the almighty God for letting me to accomplish this study. Secondly, I would like to express my heart felt gratitude to my advisor Dr. Legese Wetro, for his invaluable advices, continuous support and friendly approach through out this research. Finally, I would like to thank my family for their support during my study.

Addis Ababa University Kuba Girma
June, 2014

Introduction

Besides the basic, smooth spin down of the neutron star due to the electromagnetic torque mechanism, pulsar timing studies also reveal the presence of irregularities in the rotation of the star. The timing of radio pulsars provides us with one of the most stable clocks in the universe, even though, many pulsars exhibit a sudden increase in the spin rate, known as glitches. For instance, the young pulsars like crab pulsar glitch within a few years, however, the old pulsars do not. The question here to be raised is that, why do not the old pulsars glitch so far as the young pulsars? is not yet addressed.

A recent work reported that a total of 315 glitches were observed in 102 pulsars with fractional jumps in the spin rate ($\frac{\triangle\nu}{\nu}$) between 10^{-11} and 10^{-5} [1, 2]. Even though Anderson and Itoh suggested glitches are due to angular momentum being stored in a super-fluid component of the star that is temporarily decoupled from the charged component to which the electromagnetic emission is anchored, there is no a clear consensus on their origin yet [3]. When two components recouple, there is a sudden transfer of angular momentum to the crust, which gives the rise up of spin.

The main cause of the most glitch is the pinning of the vortices lines into the crustal lattice, which allow a lag to increase between the super-fluid and the charged component [4, 5]. A super-fluid rotates by forming a quantized array of vortices, which determines the distribution of the rotational profile of the star [3]. These quantized vortices in the neutron super-fluid in the inner crust can get pinned to the lattice of heavy neutron-rich nuclei. The pinning force is related to the energy gain when vortices are pinned to the lattice [6]. The vortices stay pinned in this manner until a stronger force unpins them

from the lattice sites. These pinned vortices in the crustal nuclei are rotating slower than the surrounding super-fluid. Due to this differential velocity, magnus forces that act radially outwards cause sudden unpinning and migration of vortices, which results in the transfer of angular momentum from the super-fluid to the crust [3]. This gives rise to a sudden speed-up of the solid crust, which manifests as a glitch in the timing behaviour of the pulsar.

In this thesis, we have shown that old pulsars show less glitches proportional to their ages and also we derived the time at which the crust and the core of neutron star will be tidally locked. The thesis is organized as follows: Chapter one talks about the formation and the structure of neutron stars, through discussing and explaining the nature of super-fluidity in neutron stars. Chapter two gives the description and explanation for the pulsar glitches by discussing vortex pinning, pinning force, Magnus force, and vortex creep. Chapter three discuss the effect of tidal interaction in neutron stars by deriving tidal force and tidal torque and based on this, we derive the time for gravitational tidal locking. Chapter four talks about the results by discussing them. Finally, we give the summary and the conclusion based on the results obtained.

Chapter 1

Neutron star

1.1 Introduction

Neutron stars are some of the densest manifestation of massive objects in the universe, which are formed by a core-collapse of supernova explosion. Their radii are between 10 and 20 kilometers and their masses are between $1M\odot$(one solar mass) and $2M\odot$. Their average masses are about $1.4M\odot$. The idea of a neutron star was first raised by Baade and Zwicky in 1934 [7]. Neutron stars have a very complicated structure [8, 9]. The first model for neutron stars structure were developed by Tolman et.al. in 1939, who applied the general theory of relativity to an ideal non-interacting neutron gas.

In this chapter, we give a brief explanation of neutron star formation, neutron star structure, pulsar discovery, and how the nature of super-fluidity in neutron star affects its rotation.

1.2 Neutron Star Formation

Neutron stars are the collapsed core of a massive star left behind after a supernova explosion. It is obvious that, a cloud in space collapses due to gravity. In the same manner the particles in a normal star feel a gravity but, do not collapse due to gravity. Because, they are balanced by the radiation pressure and gas pressure. For a massive star, the radiation pressure is produced by successive fusion of the elements of iron. If the temperature is below the fusion temperature of an available element, little contraction can raise the temperature to ignition level. A star, which has no fuel left for fusion in its core, collapses to either a white dwarf, a neutron star or a black hole depending on its mass. In a white dwarf, the gravity is balanced by the degenerate electron pressure which prevents further gravitational collapse. For a massive predecessor, the degenerate electron pressure is not sufficient to prevent a further collapse. Such a massive star will collapse to a neutron star in which degenerate neutron pressure balances gravity. If the star is to too massive for that, the star collapses to become a black hole. This event, the collapse of a massive star to a neutron star produces a supernova explosion.

1.3 Neutron Star Structure

Shapiro and Teukolsky suggested, neutron stars have a very complicated structure [9]. Even though, their structures are complicated, they are divided into atmosphere, envelope, outer crust, inner crust, outer core, and inner core.

Mass and Radius

The direct measurement of physical parameters like radius and mass of isolated neutron stars are difficult using instruments. Even though, the direct measurement is difficult, masses of neutron stars can be measured by binary dynamics in which the most accurate measurements come from binary pulsars [10]. These masses are mostly clustered very

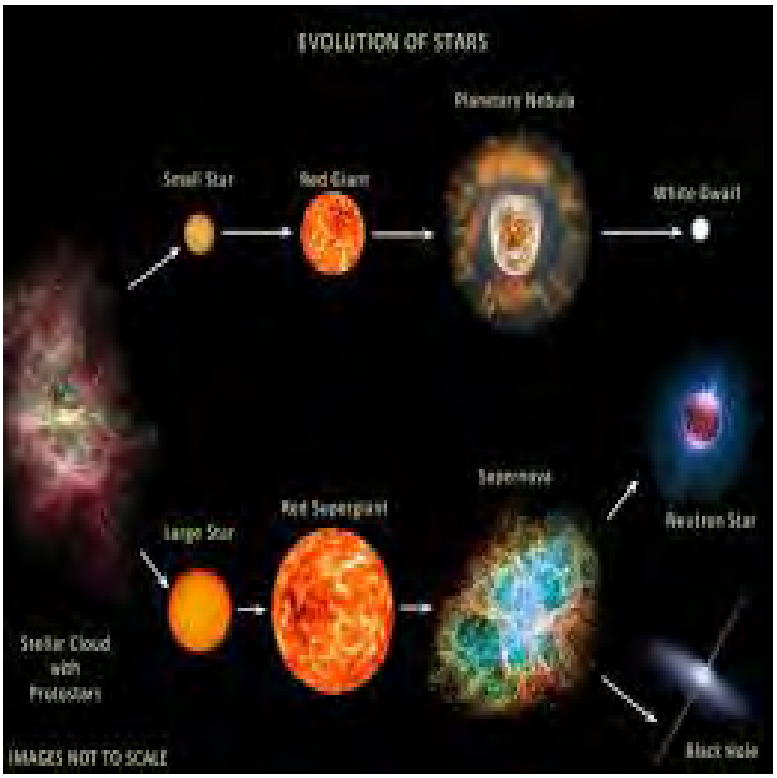

Figure 1.1: It illustrates the formation neutron star with other compact objects

strongly around $1.4M\odot$. Generally, masses of neutron stars are between $1M\odot$ and $2M\odot$ [10, 11].

Neutron stars' radii are more difficult to determine. Lattimer and Prakash suggested if the radius is greater than two times of mass of neutron star, then the object is neutron star; otherwise, it would be a black hole [10]. Another method to determine the radii and masses of neutron star is using a relevant equation of state (EOS), which relatives pressure and density with mass and radius [12]. By taking into account general relativity, the interior structures of neutron stars can be described by (with the convention G = C = 1) [13]

$$ds^2 = -e^{2\theta(r)}dt^2 + \frac{dr^2}{1-\frac{2m(r)}{r}} + r^2d\theta + r^2sin^2\theta d\phi^2. \tag{1.3.1}$$

We can determine the metric function $e^{2\theta(r)}$ and neutron stars properties by solving the following hydrostatic equations.

$$\frac{dm}{dr} = 4\Pi r^2\rho \tag{1.3.2}$$

$$\frac{dP}{dr} = -\frac{\rho m^2}{r}(1+\frac{P}{\rho})(1+\frac{4\pi Pr^3}{m})(1-\frac{2m}{r})^{-1} \tag{1.3.3}$$

$$\frac{d\theta}{dr} = -\frac{1}{\rho}\frac{dP}{dr}(1+\frac{P}{\rho})^{-1}, \tag{1.3.4}$$

Where m, ρ, and P are mass, mass density and pressure respectively. The above equations are famous Tolman-Oppenheimer-Volkoff (TOV) equations [12, 13].

Atmosphere and Envelope

Each neutron star is believed to be surrounded by an atmosphere with a thickness of around 1 cm, even though, very little is known about this region [14, 15]. Below this atmosphere, there exists a very thin region known as envelope. Gudmundsson et.al. studied the nature and the structure of neutron star's envelopes [16].

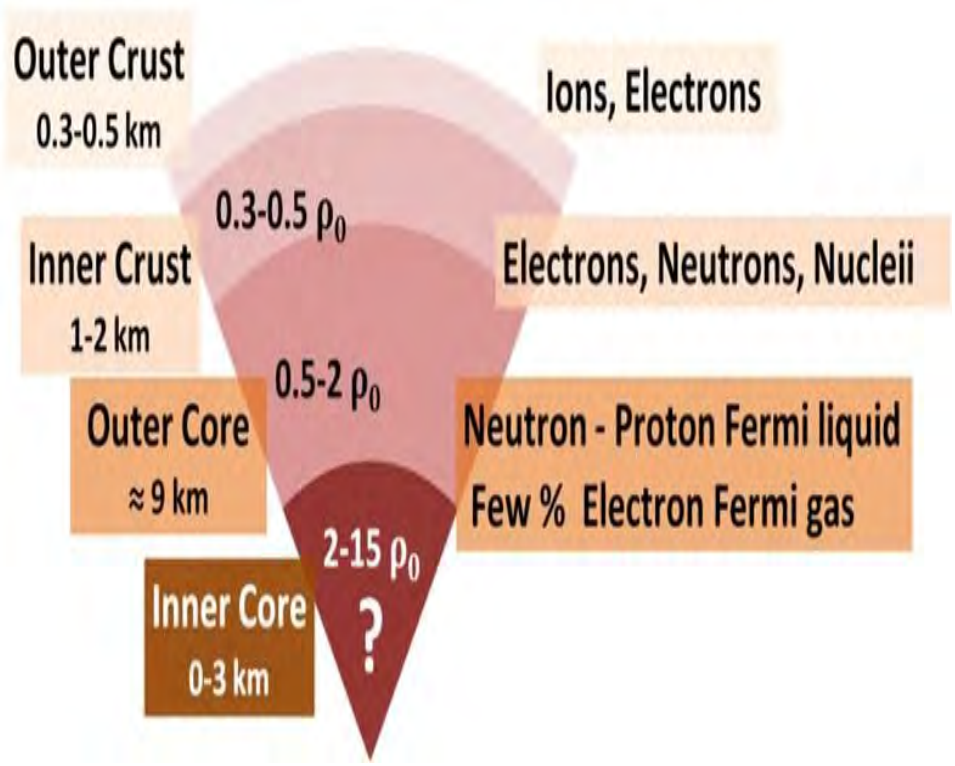

Figure 1.2: This figure illustrates the interior of neutron star with its various region thickness and density

Outer and Inner Crust

The crust of neutron star is composed by nueclei and degenerate electrons [17]. An outer layer of outer crust is made up of ^{56}Fe lattice and the structure changes rapidly with decreasing of radius, as the matter density increases. With increasing pressure and density, the electrons in this region become both degenerate and relativistic.

The inner crust contains lattices of heavier neutron-rich nuclei like ^{78}Ni, ^{76}Fe, and ^{118}Kr [18, 19]. Even though, there is no clear determination on density of crust, it is believed that density of an outer crust ranges from terrestrial densities to the neutron drip density ($\rho_{drip} \approx 4 \times 10^{11}\text{gcm}^{-3}$) and that of an inner crust ranges from neutron drip density to nuclear matter density ($\rho_o \approx 2.7 \times 10^{14}\text{gcm}^{-3}$). The region from an envelope to neutron drip density is called the outer crust.

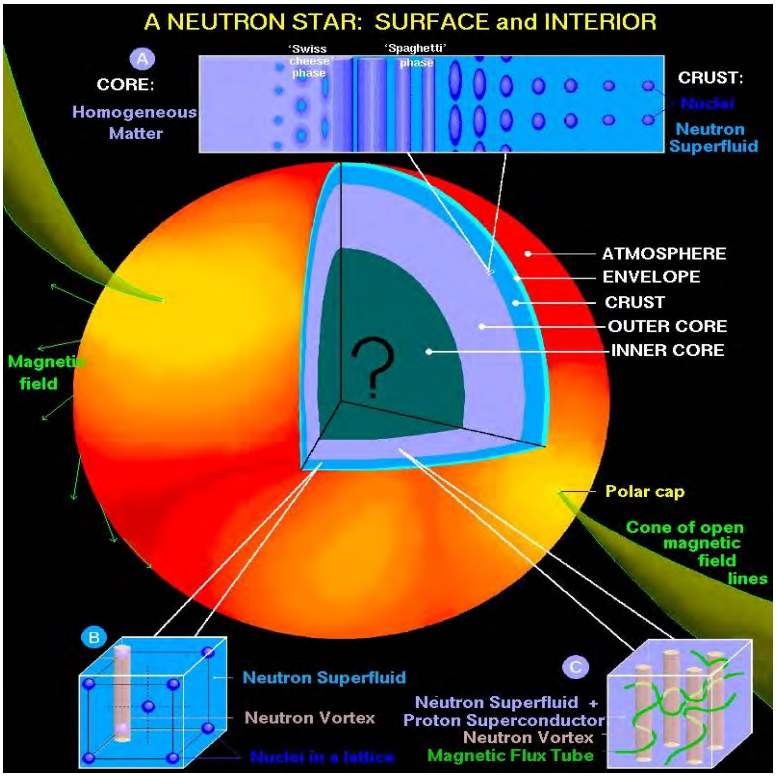

Figure 1.3: Internal composition of a neutron star. The transition from crust to core is illustrated in the top panel. In the inner crust matter is comprised of nuclei immersed in a neutron superfluid. As the density increases the protons undergo electron capture into neutrons, which then drip out of nuclei into the superfluid. In the outer core, matter is comprised of a homogeneous mixture of protons neutrons and electrons. The neutrons form a superfluid with lattice of vortex lines. The protons form a type II superconductor with magnetic flux tubes. The composition of the inner core is unknown.

Outer and Inner Core

The core of neutron star is composed by a relativistic degenerate plasma of electrons, protons, and neutrons [18]. A fluidly region, from nuclear matter density to central matter density ($\approx 10^{15} \mathrm{gcm}^{-3}$) is called the core. Even though, there is no clear hypotheses on the matters these present in the inner core, it is believed that, it contains exotic matter such as free quarks, pion, and kaon [20].

1.4 Pulsar Discovery

Pulsars are a rotating neutron stars, which are highly magnetized and rotating with high speed [21]. This is what makes differ from regular neutron stars. During their formation, they have the highest energy and fastest rotational speed. But, they slow down gradually as they release electromagnetic power through their beams.

In 1967, Jocelyn Bell, together with her supervisor, Antony Hewish, detected periodic signals while performing a galactic surve [22, 23]. At first, the sources were called LGM, an abbreviation for little green men, as they were thought to possibly be a result of extra-terrestrial communication. In fact, Hewish continued timing measurements for a few weeks to see whether there was any detectable Doppler shift due to extra-terrestrial planetary orbital motion. However, these analyses revealed no shift other than that, due to the motion of the earth. Also, soon afterwards, other sources were discovered which exhibited similarly short periods and were detected at the same radio wavelength and the idea that these radio signals were extra-terrestrial communication was abandoned [24].

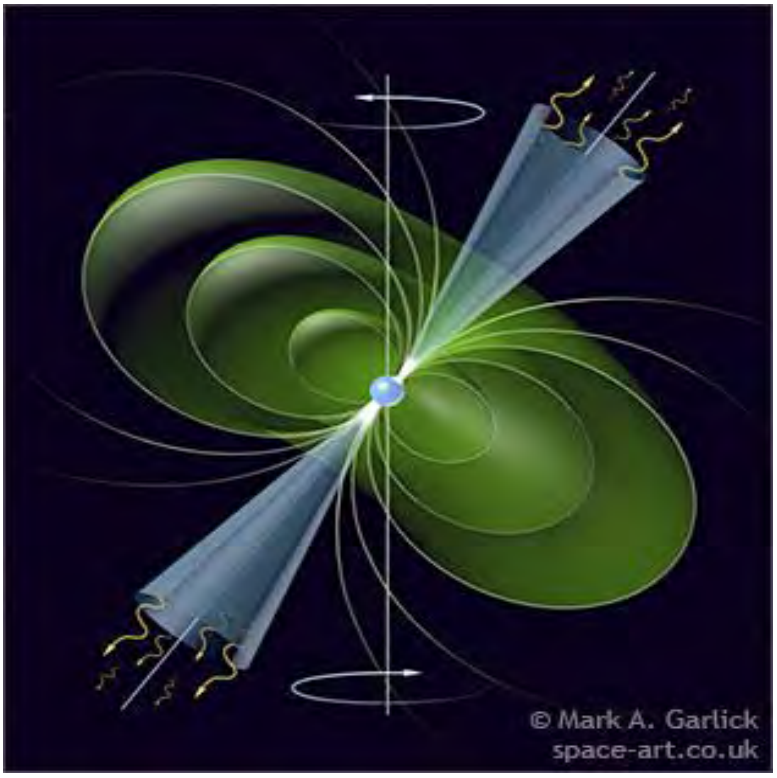

Figure 1.4: Rotating neutron star (Pulsar).

1.5 Super-fluidity in Neutron Star

The presence of super-fluidity inside neutron star was first proposed by Migdal in 1960 [25]. The bulk of the neutron star is super-fluid and it occurs in both the outer core and the inner crust, which strongly affects the behaviour of the neutron star. As the neutron star cools, it eventually reaches a critical temperature(T_c) , that will mark the onset of super-fluid formation. The value of T_c will not be constant throughout the interior of the neutron star, but rather will vary with density, pairing channel, neutron-proton asymmetries, and temperature among other factors [26].

A super-fluid is one of the realizations of a Bose Einstein Condensate and has both zero viscosity and zero entropy. The first observed super-fluid was helium II(^{4}He) [27] and most super-fluid theory has been tested, based on experimental work performed on ^{4}He. Experimentally has been shown [28] that only a small percentage of fluid helium II exists in the condensed state near absolute zero. But, the rest of the fluid exists as thermal excitations by containing the normal fluid component.

1.5.1 Basic Super-fluid Theory

A separation of a solid wall or a vortex core from the neighbour-hood causes slowly varying of super-fluid density as a function of position. As a result, macroscopic volume elements may be regarded as being of uniform density. This enables some super-fluid motions to be investigated by thermodynamic methods.

Landau described the macroscopic behaviour of the super-fluid by the means of wave function [29]. In the super-fluid, neutrons are paired together in a manner analogous to the formation of Cooper pairs in a superconductor and the paired neutrons form a boson. This enables the formation of Bose-Einstein Condensate in the fluid obtaining bosonic properties. Landau postulated that the condensate can be described by a wave function

of the following form:

$$\Psi(\mathbf{r},t) = \Psi_0(\mathbf{r},t)e^{i\phi(\mathbf{r},t)}, \tag{1.5.1}$$

which he assumed to be a solution of the Schrodinger equation. To determine the super-fluid velocity, the usual momentum operator is applied to this wave function,

$$\hat{p}\Psi = -i\hbar\nabla\Psi = \mathbf{p}\Psi. \tag{1.5.2}$$

But, a momentum is given by

$$\mathbf{p} = m\mathbf{v}_s, \tag{1.5.3}$$

where m is the mass of Cooper pair ($m = 2m_n$), and m_n is the mass of neutron. To derive the velocity of the super-fluid take $\Psi = e^{i\phi}$ and combine equation (1.5.2) and (1.5.3).

$$i\hbar\nabla e^{i\phi} = m\mathbf{v}_s e^{i\phi} \tag{1.5.4}$$

$$\mathbf{v}_s = -\frac{i\hbar}{m}\nabla(i\phi)\frac{e^{i\phi}}{e^{i\phi}}. \tag{1.5.5}$$

From equation (1.5.5), we obtain

$$\mathbf{v}_s = \left(\frac{\hbar}{m}\right)\nabla\phi, \tag{1.5.6}$$

where ϕ is the phase, and a function of position. The population density is given by

$$\Psi_0^2(\mathbf{r},t) = \frac{\rho_s}{m}. \tag{1.5.7}$$

The conservation of mass takes place in super-fluid, and described by the following continuity equation.

$$\frac{\partial}{\partial t}\rho_s + \nabla.\mathbf{j}_s = 0, \tag{1.5.8}$$

where $\mathbf{j}_s$ and ρ_s are the mass current density and the density of the super-fluid respectively. This equation is called the continuity equation for super-fluids, and describes the conservation of mass in such a fluid.

Troup obtained for large particle number N, there exists the following uncertainty relationship [30].

$$\delta N\delta\phi = 1 \tag{1.5.9}$$

As a result, N and $\hbar\phi$ can be treated as conjugate variables, in the same way as the position and momentum of a particle. Using Hamiltonian mechanics, the equations of motion for these quantities can be written as following.

$$\hbar\frac{\partial\phi}{\partial t} = -\frac{\partial H}{\partial N}, \tag{1.5.10}$$

and

$$\hbar\frac{\partial N}{\partial t} = \frac{\partial N}{\partial \phi}. \tag{1.5.11}$$

The Hamiltonian H can be given by the total energy U, consisting of the sum of the total kinetic and rest energy of the fluid.

$$U = U_k + U_0, \tag{1.5.12}$$

where U_k and U_0 are total kinetic energy and rest energy of the fluid respectively. Using mean values, the equation of motion for ϕ becomes

$$\hbar\frac{\partial\phi}{\partial t} = -\frac{\partial U}{\partial N} = -\left(\mu + \frac{1}{2}mv_s^2\right), \tag{1.5.13}$$

since the chemical potential μ is defined as

$$\mu = \left(\frac{\partial U_0}{\partial N}\right)_{entropy,volume}. \tag{1.5.14}$$

By taking the gradient of equation (1.5.13) together with (1.5.6), equation of motion for superfluid found to be

$$\hbar\frac{\partial}{\partial t}\nabla\phi = m\frac{\partial}{\partial t}v_s = -\nabla\left(\mu + \frac{1}{2}mv_s^2\right). \tag{1.5.15}$$

Next, we use conventive derivative to define Euler equation for superfluid, which is defined as

$$\frac{D}{Dt}\mathbf{a} = \frac{\partial}{\partial t}\mathbf{a} + (\mathbf{v}.\nabla)\mathbf{a}, \tag{1.5.16}$$

for an arbitrary vector a in a constant volume element traveling in a velocity field v. The Euler equation for an ideal fluid (defined as a fluid with zero viscosity, and hence applicable to a superfluid) is

$$\frac{D}{Dt}\mathbf{v}_s = \frac{\partial}{\partial t}\mathbf{v}_s + (\mathbf{v}_s.\nabla)\mathbf{v}_s = -\frac{\nabla\mu}{m}. \tag{1.5.17}$$

Using the properties of the ∇ operator, we obtain

$$\frac{D}{Dt}\mathbf{v}_s = \frac{\partial}{\partial t}\vec{v}_s + \nabla\left(\frac{1}{2}v_s^2\right) - \mathbf{v}_s \times (\nabla \times \mathbf{v}_s) = -\frac{\nabla\mu}{m} \tag{1.5.18}$$

Finally, we reach at the Landau criterion for superfluidity by comparing equation (1.5.15) with equation (1.5.17),

$$\nabla \times \mathbf{v}_s = 0, \qquad \text{if} \qquad \mathbf{v}_s \neq 0. \tag{1.5.19}$$

1.5.2 Rotating Super-fluid and Quantized Vortices

Landau's criterion has interesting implications for the rotation of the super-fluid. A rotating super-fluid carries angular momentum by forming vortex lines and the strength of this vortex is measured by circulation or vorticity around it, which is defined as

$$k = \oint_L \mathbf{v}_s.d\mathbf{l}, \tag{1.5.20}$$

for an integration contour L entirely in the super-fluid. Applying Stokes' theorem to the circulation equation and considering the Landau criterion, we get the following result.

$$k = \oint_L \mathbf{v}_s.d\mathbf{l} = \int_A (\nabla \times \mathbf{v}_s).d\mathbf{A} = 0 \tag{1.5.21}$$

This implies that, there is no circulation in a pure super-fluid, due to the constraints of the Landau criterion i.e., there is no rotation. This was famously demonstrated by the Andronikashvili experiment [31], in which an oscillating pile of disks entrained the normal fluid component, while leaving the super-fluid component at rest. However, in 1950 Osborne rotated a cylindrical bucket containing He II, and the results indicated that both the normal and super-fluid components were moving with the same angular velocity [32].

The Landau criterion tries to indicate that, it could not exist macroscopic rotation of a super-fluid and experimentally, there is no evidence for such rotation yet. However, a closer look at the theory shows that it is possible for the circulation of the super-fluid

and so does its rotation. This can be accomplished by allowing the region inside the integration contour to be multiply connected. There are two ways in which this can be accomplished. The first is to ensure that this region inside the integration contour contains holes in the super-fluid, for which $\nabla \times \vec{v_s} = 0$ i.e. holes of normal fluid. The second is to ensure that there are holes inside the integration contour which are in fact, empty of fluid. This gives rise to the concept of a vortex core. A hole in the super-fluid, having cylindrical geometry, either empty of fluid or containing normal fluid, surrounded by super-fluid matter experiencing irrotational flow once again with cylindrical symmetry.

Combining equation (1.5.6) and (1.5.20) yields the following expression for the circulation in terms of phase

$$k = \oint_L \left(\frac{\hbar}{m}\nabla\phi\right).d\mathbf{l} = \frac{\hbar}{m}\oint_L \nabla\phi.d\mathbf{l} \tag{1.5.22}$$

This becomes,

$$k = \frac{\hbar}{m}\nabla\phi. \tag{1.5.23}$$

The wave function given in equation (1.5.1) is single-valued. Thus, a complete trip around the contour should yield an unchanged value. So, due to the nature of the wave function, the only possible values for a change in ϕ are multiples of 2π and zero. Obviously, a value of zero corresponds to the Landau criterion and the multiples of 2π give non-zero circulation, which apply to the case of vortices. In this case, the circulation is given by

$$k = n\frac{\hbar}{m}, \tag{1.5.24}$$

where n is an integer. Thus, the circulation is quantized.

It is from the above conceptual framework that the definition of a vortex core is obtained; a vortex core is the non-super-fluid region found inside a vortex, i.e. the region in which $\nabla \times \mathbf{v_s} = 0$. Although, super-fluid rotation cannot occur in a simply connected region, it can occur macroscopically in the presence of the many multiply connected regions formed by quantized vortex lines.

Considering a streamline located at radius r from the center of an isolated vortex line, the following equation applies

$$k = \oint_L \mathbf{V}_s . d\mathbf{l} = 2\pi r v_s(r). \tag{1.5.25}$$

Hence, the velocity of the fluid at a given distance from the vortex core is

$$\mathbf{v}_s = \frac{\mathbf{k}}{2\pi r} = \frac{n\hbar}{m}, \tag{1.5.26}$$

and the angular momentum at that point is

$$\mathbf{L} = m\mathbf{v}_s r = n\hbar. \tag{1.5.27}$$

Thus, in addition to the circulation, both the velocity and angular momentum of the fluid around a vortex line are quantized.

The first experimental evidence of quantized circulation was recorded by Vinen [33] while the existence of quantized vortices in He II was shown by Hall and Vinen [34]. This theory was first related to neutron stars by Ginzburg and Kirzhnits in 1964 [35] when they stated that, should rapidly rotating neutron stars exist, then quantized vortices similar to those observed in He II should exist in the neutron super-fluid of these compact bodies. These predictions were made before the discovery of pulsars and their interpretation as rapidly rotating neutron star.

Chapter 2

Pulsar Glitches

2.1 Introduction

Pulsars are characterized by the remarkable stability of their pulsation frequency. However, the pulse arrival times occasionally exhibit some striking irregularities [36]. These irregularities fall into two categories: timing noise and glitches.

Glitches are a sudden increasing or decreasing of the rotational frequency of a pulsar [37]. Their origin is still debated and the giant spin-ups observed in the 20 known vela-like glitchers could indicate the presence of bulk super-fluidity inside these stars [2]. This giant glitches would represent the natural macroscopic outcome of the interaction between quantized neutron vortex lines, which carry the angular momentum of the rotating chargeless superfluid [38]. This interaction can pin vortices to the normal component of the star, and freezing the super-fluid vorticity by storing its angular momentum. When the hydrodynamical lift on a vortex (magnus force) equals with the pinning force on a line, the angular momentum can transfer to the normal component of the star by the action of drag force. According to Anderson and Itoh [3], giant glitches are due to the sudden and simultaneous depinning of a large number of accumulated vortices, followed by the rapid transfer of their angular momentum to the observable normal crust.

In this chapter we give the description and explanation of the cause for glitches (vortex pinning and vortex creeping) through the discussion of pinning force, magnus force, and post-glitches relaxation detaily.

2.2 Glitches: Vortex Pinning

The observed glitches in the pulsation periods of neutron stars are thought to be manifestations of neutron super-fluidity in the inner crust of neutron stars [3]. The inner crust is the region of the star, where bloated neutron-rich nuclei coexists with a free neutron gas. Through out the inner crust a free neutron pair produce an isotropic super-fluid whose interaction with the nuclei in the crust is, proposed to regulate the glitch of the star. The super-fluid and nuclei interact predominantly via vortex lines to thread those rotating super-fluid. The lines are either attract to or repel from nuclei depending on the local density. In either case the energy of a vortex line is minimized if its path through the nuclear lattice is optimally chosen and it is thereby pinned to the crust. If all the vortex lines were pinned, the angular velocity of the super-fluid would be fixed.

Magnetic braking at the surface of the star slows the rotation of stellar crust. But, cannot alter the angular velocity of the super-fluid unless the vortex lines are displaced or new ones are created. Since pinning prevents the lines from moving and nucleation, it requires either high temperatures or large velocity gradient. The super-fluid velocity does not decrease as rapid as that of the crust, and it develops a velocity difference between the super-fluid and the crust. This a velocity difference causes as a source of pulsar glitches.

2.2.1 Equations of Motion of Vortex Lines in the Inner Crust

We consider the motion of vortex lines in an inner crust, where the lattice nuclei are embedded in a super-fluid of neutron sea. We adopt the cartesian coordinates fixed in the rest frame of the lattice nuclei. The $z-axis$ is chosen to be parallel to one of the major axes of a body-centered cubic lattice. we can describe their motion and configurations by the two-dimensional position vectors, $\mathbf{u} = (x, y)$, of vortex lines in the x-y plane which depend on the coordinate z. The equation of motion of vortex lines is written as

$$\mathbf{F}_p + \rho\mathbf{k} \times (\frac{\partial \mathbf{u}}{\partial t} - \mathbf{v}_s) + T\frac{\partial^2 \mathbf{u}}{\partial z^2} = 0 \tag{2.2.1}$$

where ρ is the superfluid density, $\mathbf{F}_p$ the pinning force perunit length of a vortex line, $\mathbf{k}$ the circulation of a vortex, $\mathbf{v}_s$ the locally uniform superfluid velocity, and T the tension of the vortex line. Vortices in the superfluid are quantized. Each vortex line carries one quantum $k = \frac{h}{m}$ of circulation, where h is the Planck's constant and m is the mass of a Cooper pair, which is twice of a neutron mass m_n . Since we consider the vortex lines aligned or almost aligned with the z-axis, we approximate the circulation vector by

$$\mathbf{k} = \frac{h}{m}\hat{z} \tag{2.2.2}$$

where $\hat{z}$ is the unit vector along the z-axis. In the vortex unpinning model the difference in angular velocity between the inner crust superfluid and the crust is reduced significantly just after the glitches, decoupling the inner crust superfluid from the crust. As the crust is slowed down by the external braking torque, the angular velocity difference $\triangle\mathbf{\Omega}$ builds up between the local superfluid and the lattice nuclei. Using the glitch interval t_g and the angular deceleration rate $\dot{\mathbf{\Omega}}$, the angular velocity difference just before the glitch is estimated as

$$\triangle\mathbf{\Omega} \approx |\dot{\mathbf{\Omega}}|t_g. \tag{2.2.3}$$

The third term in equation (2.2.1) comes out from the tension of vortices when vortices are distorted from the straight lines. The energy of vortex lines is equal to the kinetic

energy of the velocity eld induced by them. The tension is given by the energy per unit length

$$T = \rho k c_k, \tag{2.2.4}$$

where the parameter c_k is only logarithmically dependent on the wave number and the neutron superfluid coherence length [39]. The vortex-nucleus interaction has an attractive component arising from the change in the condensation energy and a repulsive component arising from the change in kinetic energy of circulating superfluid. The interaction potential is given by

$$V = -E_p e^{-\frac{u^2}{2\xi^2}}, \tag{2.2.5}$$

where E_p is the pinning energy (or the interaction energy) per nucleus, ξ is the vortex core radius or the coherence length of the neutron superfluid, and u is the distance in the x-y plane between the nucleus and the vortex line, $u^2 = x^2 + y^2$. The coherence length of the neutron superfluid is written as

$$\xi = \frac{2E_F}{\pi k_F \triangle}, \tag{2.2.6}$$

where $\triangle$ is the energy gap for the superfluid neutrons, E_F their Fermi energy, and k_F the Fermi surface wave number. We can obtain the lattice-vortex interaction potential by summing the above potential in equation (2.2.5), which is contributed from each nucleus over the entire nuclei of a single large crystal.

2.2.2 Pinning Force

Although vortex pinning in the crust has been suggested as the main mechanism behind pulsar glitches more than 20 years ago by Anderson and Itoh [3], until recently very little work has been devoted to obtaining realistic estimates of the pinning force. The main difficulty lies in the fact that, although there have been several estimates of the pinning energy and thus of the force per pinning site [40], it is in fact the pinning force per unit

length acting on a vortex that is the relevant quantity to compare with the magnus force if one is to understand when a vortex line can unpin [41].

In fact it has been argued by Jones [42] that if one considers an infinitely long vortex line and averages over the various orientations with respect to the lattice, the pinning force will be negligible. Recent calculations by Grill [43] have shown that for realistic configurations in which one considers a vortex to be rigid over length-scales of 100-1000 Wigner-Seitz radii, the averaging process over microscopic length-scales and different orientations of the lattice does indeed reduce the strength of the pinning force with respect to previous estimates based on the pinning force per pinning site. However, the values obtained in these calculations, which are in fact the first realistic estimate of the pinning force per unit length, are still large enough to explain pulsar glitches [44]. The pinning force, which acts to pin the vortex line to nuclei, per site is approximately given by

$$\mathbf{F}_p = \frac{E_p}{\xi} \tag{2.2.7}$$

where E_p is the pinning energy (or the interaction energy) per nucleus, ξ is the vortex core radius or the coherence length of the neutron superfluid.

2.2.3 Magnus Force

A vortex line would tend to move with the ambient superfluid, unless there is some force in the system which acts to prevent this. This ambient superfluid moves with its own angular velocity Ω_s. However, the vortex lines pinned to the crustal nuclei and move with the solid crust, which generally moves at a lower angular velocity Ω_{cr}. This happens due to the electromagnetic torques, which slow down a rotation of pulsar by acting directly on the crust. Thus, it is Ω_{cr} that is to be identified with the observed angular velocity of the star, since pulsar emission processes are believed to be related to the external surface of the solid crust, and the magnetic field threading through it. Ω_s always lags behind it.

Because of this difference of velocities between a vortex line and its ambient superfluid, the former is acted upon by a force which is called the magnus force. This would neutralize the difference of velocity between the crust and the super-fluid. In equation (2.5.1) the second term represents the magnus force, which arises when the relative motion exists between the local superfluid and the vortex. The magnus force acting on a unit length of a vortex line is given by

$$\mathbf{F}_m = \rho \mathbf{k} \times (\mathbf{v}_v - \mathbf{v}_s), \tag{2.2.8}$$

where $\mathbf{v}_v$ is the vortex's velocity.

2.3 Post-Glitch Relaxation: Vortex Creep

Between glitches, the vortex lines are believed to undergo a slow, thermally activated process called vortex creep, which is a quantum tunneling between adjacent sites and geometrically suitable for pinning. In this condition, the creeping process approaches to a steady state when it left to itself, but a glitch perturbs it away from this steady state. This process of recoupling of the vortex creep to another steady state is called post-glitch relaxation.

The superfluid dynamics must be considered when analysing the post-glitch recovery described by the two-component model. In the steady state the superfluid lags the crust. Vortices in the superfluid component steadily creep outwards, in a similar fashion to dislocate hopping through a crystal lattice. The steady-state lag depends on the limiting creep rate, which in turn depends on the pinning strength of vortices in the crust and so does the temperature of the star [45]. The lag never disappears, i.e., there is a superfluid angular momentum reservoir. Pulsar glitches never deplete this reservoir; only small fractions of it build up and relax away, hence there is no observed correlation between glitch sizes and waiting times [1].

Alpar et.al., attempted to explain the recovery of the first eight glitches in the vela

pulsar in terms of vortex creep [46]. They divided the star into multiple components, representing regions of the star with different pinning strengths. Where the temperature is large compared with the pinning strength, the dynamical response $\Omega(t)$ is exponential decay($linear$); elsewhere, the response is more complicated ($non-linear$). By fitting the model to observations, the moments of inertia corresponding to the regions of different pinning strengths are identified, where the shorter two time-scales follow a linear response, while the longer is nonlinear. The initial angular velocity of each region of the star is also extracted.

Sedrakian and Hairapetian reconsidered the vortex creep picture by modelling the motion of vortices in the superfluid during glitch relaxation [47]. The vortices migrate at a rate which depends on the time-scales for pinning and unpinning. By fitting the model to the observed relaxation in the first eight glitches of the vela pulsar, the general features of the vortex distribution immediately after a glitch are determined. It is found that the short relaxation time-scale observed ($\sim 10h$) arises from the motion of vortices initially contained within large radii ($9.57km$ for a star of total radius $9.61km$), while the longer time-scales ($3.2d$ and $32d$) are confined to smaller radii ($9.53km$ and $9.47km$ respectively). The region of the star responsible for steady-state relaxation is confined within a radius $9.36km$, while vortices at smaller radii result in unobservable relaxation times.

The vortex creep model developed for vela cannot account for the overshoot observed in the post-glitch relaxation of the crab pulsar. Alpar et.al., proposed that the glitches in the crab arise from starquake-driven vortex unpinning, as opposed to magnus force driven unpinning in Vela [46]. The overshoot arises from vortex migration inwards into newly formed vortex traps created during the quake, while the long-term response is due to vortex migration similar to that expected in Vela [46]. The dynamical response then comprises two linear components (the short time-scales) and the non-linear response (long-term recovery) with time-scales $\sim 0.8h, 12d$ and $200d$.

Vortex creep theory models the dynamical behaviour of the neutron star in terms of perturbations and relaxation of the thermal flow of quantized vortex lines, whose distribution determines the dynamics of a pinnned superfluid in the neutron star's crust. The origin of the glitches themselves is attributed to a sudden unpinning of vortex lines resulting in a decrease $\delta\mathbf{\Omega}_s$ in the rotation rate of the superfluid a corresponding increase $\triangle\mathbf{\Omega}_{cr}$ in the rotation rate of the star's crust. By angular momentum conservation,

$$\triangle\mathbf{\Omega}_{cr} = \frac{I_p}{I_{cr}}\delta\mathbf{\Omega}_s, \tag{2.3.1}$$

where I_p is the moment of inertia of the pinned superfluid involved in the glitch and I_{cr} is the effective moment of inertia of the crust. I_{cr} is effectively the total moment of inertia, I of the neutron star as the bulk of the star rotates rigidly with the crust on time-scales of interest [48].

In applications of vortex creep theory, the pinned superfluid does not recouple to the slow down of the star for an off set time t_0 following the glitch:

$$t_0 = \frac{\delta\mathbf{\Omega}_s}{|\dot{\mathbf{\Omega}}|} \qquad \text{or} \qquad t_0' = \frac{\triangle\mathbf{\Omega}_{cr}}{|\dot{\mathbf{\Omega}}|}, \tag{2.3.2}$$

where the former expression refers to the regions of superfluid through which vortex moved during the glitch and the latter to regions through which no vortex motion took place.

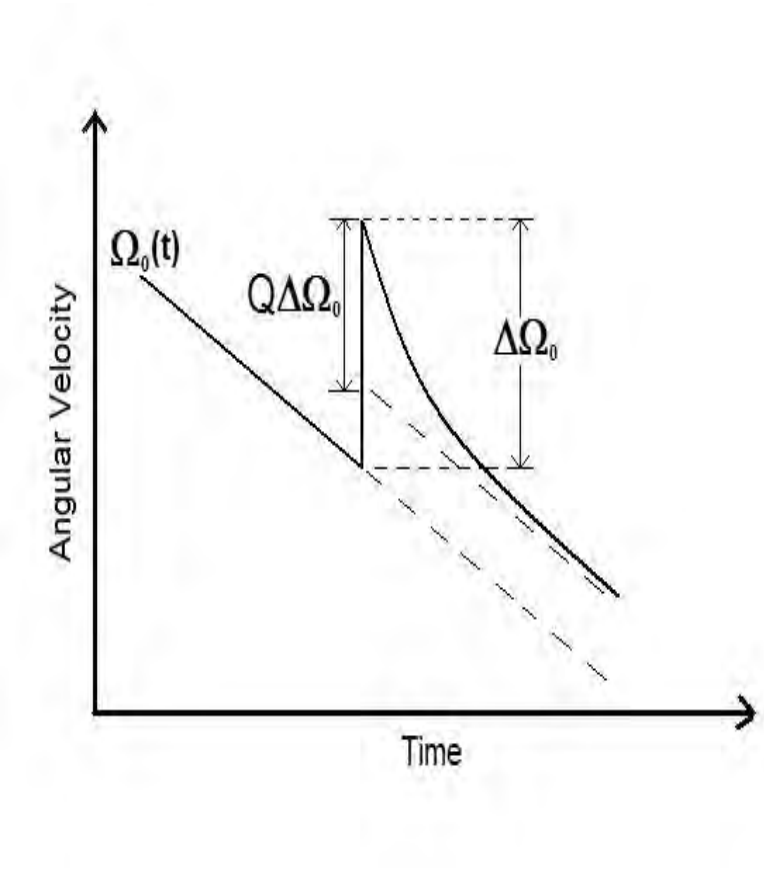

Figure 2.1: Pulsar angular frequency versus time for a typical glitches. The recovery typically takes days to weeks. The recovery fraction Q measures the proportion of $\triangle\Omega$ which decays.

2.3.1 Regimes of Vortex Creep

The equation of motion for the rotation rate $\mathbf{\Omega}_s$ of any uniformly rotating superfluid can be written as

$$\dot{\mathbf{\Omega}}_s = -2\mathbf{\Omega}_0 \frac{v_v}{r}, \tag{2.3.3}$$

where $\mathbf{\Omega}_0$ is a constant reference value of $\mathbf{\Omega}_s$ and v_v is the mean velocity of the vortex lines in the radially outward direction. The superfluid in the inner crust of the neutron star coexists with a lattice, which pins the vortex lines with typical pinning energies E_p at each pinning site. Hence, the motion of the vortex lines and the rotation rate of the superfluid are constrained as a result of pinning. A lag $\omega \equiv \mathbf{\Omega}_s - \mathbf{\Omega}_{cr}$ ensues between the superfluid's rotation rate and the neutron star's crust. A given pinning energy E_p can support at most a critical lag ω_{cr}, at which vortices will unpin. At a finite temperature T, there will be a mean thermal *creep* of vortices in the radially outward direction as the star is spun down by external torques. This vortex creep makes the superfluid couple to the spin down of the crust and with simple considerations leads to [49]

$$v_v = 2v_0 exp\left(\frac{-E_p}{kT}\right) sinh\left(\frac{E_p}{kT}\frac{\omega}{\omega_{cr}}\right). \tag{2.3.4}$$

Here v_0 is a typical microscopic velocity of the vortex lines, which is the order of 10^7cm s^{-1} and k is the Boltzmann constant. Equations (2.3.3) and (2.3.4) are supplemented by an equation of motion for the rotation rate $\mathbf{\Omega}_{cr}$ of the crust:

$$I_{cr}\dot{\mathbf{\Omega}}_{cr} = N_{ext} - I_p\dot{\mathbf{\Omega}}_s \equiv (I_p + I_{cr})\dot{\Omega}_\infty - I_p\dot{\mathbf{\Omega}}_s \equiv I\dot{\Omega}_\infty - I_p\dot{\mathbf{\Omega}}_s, \tag{2.3.5}$$

where N_{ext} is the external torque and $\dot{\Omega}_\infty$ denotes the steady- state value of both $\dot{\mathbf{\Omega}}_{cr}$ and $\dot{\mathbf{\Omega}}_s$ and we have included a single superfluid component in the above.

We note that vortex creep will have a linear or non-linear depending on the lag ω, according to the value of

$$sinh\left(\frac{E_p}{kT}\frac{\omega}{\omega_{cr}}\right) \cong \frac{|\dot{\mathbf{\Omega}}_{cr}|}{4\mathbf{\Omega}_0}\frac{r}{v_0} exp\left(\frac{E_p}{kT}\right) = \frac{r}{8t_{sd}v_0} exp\left(\frac{E_p}{kT}\right) \tag{2.3.6}$$

If the pulsar's spin down age $t_{sd} = \Omega/(2|\dot{\mathbf{\Omega}}_{cr}|)$ is short enough or the pinning strong enough compared to kT, one can take

$$sinh\left(\frac{E_p}{kT}\frac{\omega}{\omega_{cr}}\right) \cong \frac{1}{2}exp\left(\frac{E_p}{kT}\right), \tag{2.3.7}$$

while in the opposite limit of weak enough pinning or long enough spin down age, the dependence on ω is linear. The exponential dependence of creep on perturbations of the lag ω lead to almost complete stop of vortex creep. Regions of the superfluid those are in the non-linear regime will experience a complete decoupling from the crust until a time t_0 or t_0', when creep stars again.

In contrast, if the region of vortex creep is warranted, a very simple dynamical model ensues:

$$\dot{\mathbf{\Omega}}_s = -\frac{2\Omega_0 v_0}{r}exp\left(\frac{-E_p}{kT}\right)\frac{E_p}{kT}\frac{\omega}{\omega_{crit}} \equiv -\frac{\omega}{\tau} = -\frac{(\Omega_s - \Omega_{cr})}{\tau}, \tag{2.3.8}$$

where

$$\tau = \frac{r\omega_{crit}}{2\Omega_0 v_0}\frac{kT}{E_p}exp\left(\frac{E_p}{kT}\right). \tag{2.3.9}$$

An important difference between the two creep regimes lies in the steady-state value ω_∞ of the lag. In the exponential regime [49],

$$\omega_\infty = \omega_{crit}\left[1 - \frac{kT}{E_p}ln\left(\frac{2v_0 t_{sd}}{r}\right)\right] \cong \omega_{crit}. \tag{2.3.10}$$

ω_{crit} is estimated to be the order of 10^{-1}, with an observational upper limit $\bar{\omega}_{cr} \lesssim 0.7$ for its average value [50]. By contrast, the lag in the linear regime is much smaller,

$$\omega_\infty = |\dot{\mathbf{\Omega}}|_\infty \tau \tag{2.3.11}$$

Chapter 3

Tidal Interaction in Neutron Star

3.1 Introduction

An exciting prospect for gravitational waves detection, is provided by the chance to extract information about the neutron star equation of state from the inspiral part of the signal. As the binary spirals inward, the neutron star experience ever increasing tidal forces from the gravitational field of the companion object. In many cases the strong tidal interaction may cause the star disruption, before it begins the final plunge into the black holes horizon or the merger with another neutron star.

In this chapter, we discuss the effect of tidal interaction in neutron stars by deriving tidal force and tidal torque and also based on this, we derive the time for gravitational tidal locking.

3.2 Newtonian Tidal Forces

The Newtonian tidal tensor is a useful tool for the study of tidal fields. To deal with tidal fields, first let us derive the tidal force tensor. We consider a cartesian coordinate system that is in free-fall in a gravitational field. Define Φ such that the function of potential energy V, which has a value $V = m\Phi$, where m is the gravitational mass of the test

particle. The gravitational force $\mathbf{F}_g$ is given as

$$\mathbf{F}_g = -\nabla V = -\nabla(m\Phi) = \frac{d\mathbf{P}}{dt}$$

$$-m(\nabla\Phi) = \frac{d}{dt}(m\mathbf{v}) = m\mathbf{g}$$

$$\mathbf{g} = -\nabla\Phi, \tag{3.2.1}$$

where $\mathbf{g}$ is the acceleration of the particle due to gravity. We can write equation (3.2.1) in another form as

$$\mathbf{g} = -\nabla\Phi = -\sum_{k=1}^{3} \frac{\partial\Phi}{\partial x^k}\hat{\mathbf{e}_k}, \tag{3.2.2}$$

where $\hat{\mathbf{e}_k}$ is a unit vector and $k = 1, 2, 3$.

The difference in gravitational acceleration of a test particle $d\mathbf{g}$ relative to a reference point in free-fall is given by

$$d\mathbf{g} = -d\left(\sum_k \frac{\partial\Phi}{\partial x^k}\hat{\mathbf{e}_\mathbf{k}}\right)$$

$$d\mathbf{g} = -d\left(\sum_j \left(\frac{\partial x^j}{\partial x^j}\right)\sum_k \frac{\partial\Phi}{\partial x^k}\hat{\mathbf{e}_\mathbf{k}}\right)$$

$$d\mathbf{g} = -\sum_j \frac{\partial}{\partial x^j}\left(\sum_k \frac{\partial\Phi}{\partial x^k}\right) dx^j\hat{\mathbf{e}_\mathbf{k}}$$

$$d\mathbf{g} = -\sum_{j,k} \frac{\partial}{\partial x^j}\left(\frac{\partial\Phi}{\partial x^k}\right) x^j\hat{\mathbf{e}_\mathbf{k}}$$

$$d\mathbf{g} = -\sum_{j,k} \frac{\partial^2\Phi}{\partial x^j\partial x^k} x^j\hat{\mathbf{e}_\mathbf{k}}. \tag{3.2.3}$$

Using equation (3.2.3), the tidal force tensor $\mathbf{F}_t$ is written as

$$\mathbf{F}_t = m d\mathbf{g} = -m\sum_{j,k} \frac{\partial^2\Phi}{\partial x^j\partial x^k} x^j\hat{\mathbf{e}_\mathbf{k}}$$

$$\mathbf{F}_t = -m\sum_{j,k} T_{jk}x^j\hat{\mathbf{e}_\mathbf{k}}, \tag{3.2.4}$$

where the quantity T_{jk} $(j,k=1,2,3)$ is the component of the tidal force tensor and has a value of

$$T_{jk} = \frac{\partial^2 \Phi}{\partial x^j \partial x^k}. \tag{3.2.5}$$

The tidal force tensor is a cartesian, hence the term T_{jk} is a cartesian tensor and let see how it transforms under an orthogonal transformation. We start by taking the derivative of the scalar Φ and using the chain rule.

$$\frac{\partial \Phi}{\partial x^k} = \frac{\partial x^n}{\partial x^k}\frac{\partial \Phi}{\partial x^n} = \delta^n_k \frac{\partial \Phi}{\partial x^n}, \tag{3.2.6}$$

where $\delta^n_k = \frac{\partial x^n}{\partial x^k} = constant$. By taking the derivative of equation (3.2.6) with respect to $x^{j'}$, we get

$$\begin{aligned}
\frac{\partial}{\partial x^{j'}}\left(\frac{\partial \phi}{\partial x^k}\right) &= \frac{\partial}{\partial x^{j'}}\left(\delta^n_k \frac{\partial \Phi}{\partial x^n}\right) \\
\frac{\partial^2 \Phi}{\partial x^{j'} \partial x^{k'}} &= \frac{\partial x^m}{\partial x^j}\frac{\partial}{\partial x^m}\left(\delta^n_k \frac{\partial \Phi}{\partial x^n}\right) \\
T'_{jk} &= \delta^m_j \delta^n_k \left(\delta^n_k \frac{\partial \Phi}{\partial x^n}\right) \\
T'_{jk} &= \delta^m_j \delta^n_k T_{mn}.
\end{aligned} \tag{3.2.7}$$

Thus, the quantities T_{jk} is the covariant components of a cartesian tensor. The differential component of the tidal force has the following forms, using Einstein's summation convention.

$$\begin{aligned}
dF_{tx_j} = \frac{\partial F_{g_j}}{\partial x^k} dx^k &= -m \frac{\partial^2 \Phi}{\partial x^j \partial x^k} dx^k \\
dF_{tx_j} &= -m T_{jk} dx^k
\end{aligned} \tag{3.2.8}$$

In the next sections it is useful to discuss the main concepts associated with the most typical tidal perturbation that induced by the spherical potential of a point mass $\Phi^{\alpha\beta}(r) = \frac{GM}{r}$ [51]. Since, it is a real symmetric matrix, there must be a frame of reference for which $T^{\alpha\beta}$ is diagonal. If we choose a frame of reference where the z-axis passes through the particles position corresponding to the radial spherical coordinate, that is $(x^1 = x =$

$0, x^2 = y = 0,\ x^3 = z = r)$, then T_{jk} is diagonal and becomes

$$T^{\alpha\beta}_{jk} = \begin{pmatrix} \frac{GM}{r^3} & 0 & 0 \\ 0 & \frac{GM}{r^3} & 0 \\ 0 & 0 & \frac{-2GM}{r^3} \end{pmatrix} = \frac{GM}{r^3}\begin{pmatrix} 1 & 0 & 0 \\ 0 & 1 & 0 \\ 0 & 0 & -2 \end{pmatrix} \tag{3.2.9}$$

From equation (3.2.8), each components of tidal force can be written as

$$dF^{\alpha\beta}_{tx} = -mT^{\alpha\beta}_{xx}dx = -\frac{GMm}{r^3}dx \tag{3.2.10}$$

$$dF^{\alpha\beta}_{ty} = -mT^{\alpha\beta}_{yy}dy = -\frac{GMm}{r^3}dy \tag{3.2.11}$$

$$dF^{\alpha\beta}_{tz} = -mT^{\alpha\beta}_{zz}dz = \frac{2GMm}{r^3}dz, \tag{3.2.12}$$

where

$$T^{\alpha\beta}_{xx} = T^{\alpha\beta}_{yy} = \frac{GM}{r^3} \qquad \text{and} \qquad T^{\alpha\beta}_{zz} = -\frac{2GM}{r^3}. \tag{3.2.13}$$

The tidal force given by equation (3.2.10), (3.2.11) and (3.2.12) satisfies the identity

$$\frac{\partial F_{tx}}{\partial x} + \frac{\partial F_{ty}}{\partial y} + \frac{\partial F_{tz}}{\partial z} = -\frac{GMm}{r^3} - \frac{GMm}{r^3} + \frac{2GMm}{r^3} = 0, \tag{3.2.14}$$

that is the tidal force has zero divergence. This result hold in general for gravitational field in empty region of space and we can prove it as

$$\frac{\partial}{\partial x^k}F^k_t = -\frac{\partial}{\partial x^k}\left(m\frac{\partial^2\Phi}{\partial x^j \partial x^k}x^j\right)$$

$$\frac{\partial}{\partial x^k}F^k_t = -m\frac{\partial x^j}{\partial x^k}\frac{\partial^2\Phi}{\partial x^j \partial x^k}$$

$$\frac{\partial}{\partial x^k}F^k_t = -m\delta^j_k\frac{\partial^2\Phi}{\partial x^j \partial x^k}$$

$$\frac{\partial}{\partial x^k}F^k_t = -m\delta^j_j\frac{\partial^2\Phi}{\partial x^k \partial x^k}$$

$$\frac{\partial}{\partial x^k}F^k_t = 0, \tag{3.2.15}$$

where

$$\delta^j_j = 1 \qquad \text{and} \qquad \frac{\partial^2\Phi}{\partial x^j \partial x^j} = 0, \tag{3.2.16}$$

because Φ is a constant. Equation (3.2.15) hold true because in empty space the gravitational potential satisfies the laplace equation. But in the presence of a mass density ρ, the divergence of the tidal force is given by

$$\frac{\partial}{\partial x^k} F_t^k = -4\pi m G\rho \tag{3.2.17}$$

3.3 Relativistic Tidal Forces

Relativistic tidal force is force acted on the motion of free particles due to gravitational waves. Let consider the relative motion of two nearby test particles in free fall to understand the effect of gravitational waves. To do this, let first calculate the first and second derivative of a vector field(call it $\mathbf{A}^\mu$) along geodesic curve, since the free test particles obey the geodesic equation.

$$\begin{aligned}\frac{DA^\mu}{D\tau} &= \frac{dx^\nu}{d\tau}\frac{dA^\mu}{dx^\nu} = A^\mu{}_{;\nu}\frac{dx^\nu}{d\tau} \\ &= \frac{dA^\mu}{d\tau} + \Gamma^\mu_{\alpha\beta}A^\alpha\frac{dx^\beta}{d\tau}.\end{aligned} \tag{3.3.1}$$

Now we can calculate the second derivative of A^μ using equation (3.3.1)

$$\frac{D^2A^\mu}{D\tau^2} = \frac{d}{d\tau}\frac{DA^\mu}{D\tau} + \Gamma^\mu_{\alpha\beta}\frac{DA^\alpha}{D\tau}\frac{dx^\beta}{d\tau}. \tag{3.3.2}$$

By substituting equation (3.3.1) into equation (3.3.2), we obtain

$$\frac{D^2A^\mu}{D\tau^2} = \frac{d}{d\tau}\left(\frac{dA^\mu}{d\tau} + \Gamma^\mu_{\alpha\beta}A^\alpha\frac{dx^\beta}{d\tau}\right) + \Gamma^\mu_{\alpha\beta}\frac{DA^\alpha}{D\tau}\frac{dx^\beta}{d\tau}. \tag{3.3.3}$$

Expanding equation (3.3.3) gives

$$\frac{D^2A^\mu}{D\tau^2} = \frac{d^2A^\mu}{d\tau^2} + \frac{d}{d\tau}\left(\Gamma^\mu_{\alpha\beta}A^\alpha\frac{dx^\beta}{d\tau}\right) + \Gamma^\mu_{\alpha\beta}\left(\frac{dA^\alpha}{d\tau} + \Gamma^\alpha_{k\lambda}A^k\frac{dx^\lambda}{d\tau}\right)\frac{dx^\beta}{d\tau}. \tag{3.3.4}$$

Further more expanding equation (3.3.4) results

$$\frac{D^2A^\mu}{D\tau^2} = \frac{d^2A^\mu}{d\tau^2} + \left(\frac{d}{d\tau}\Gamma^\mu_{\alpha\beta}\right)A^\alpha\frac{dx^\beta}{d\tau} + \Gamma^\mu_{\alpha\beta}\left(\frac{dA^\alpha}{d\tau}\right)\frac{dx^\beta}{d\tau} + \Gamma^\mu_{\alpha\beta}A^\alpha\frac{d}{d\tau}\left(\frac{dx^\beta}{d\tau}\right)$$

$$+\Gamma^{\mu}_{\alpha\beta}\frac{dA^{\alpha}}{d\tau}\frac{dx^{\beta}}{d\tau}+\Gamma^{\mu}_{\alpha\beta}\Gamma^{\alpha}_{k\lambda}A^{k}\frac{dx^{\lambda}}{d\tau}\frac{dx^{\beta}}{d\tau}. \tag{3.3.5}$$

Rearranging equation (3.3.5) gives

$$\begin{aligned}\frac{D^2A^{\mu}}{D\tau^2}=\frac{d^2A^{\mu}}{d\tau^2}+\frac{d}{dx^{\nu}}\Gamma^{\mu}_{\alpha\beta}\frac{dx^{\nu}}{d\tau}A^{\alpha}\frac{dx^{\beta}}{d\tau}+\Gamma^{\mu}_{\alpha\beta}\frac{dA^{\alpha}}{d\tau}\frac{dx^{\beta}}{d\tau}+\Gamma^{\mu}_{\alpha\beta}A^{\alpha}\frac{d^2x^{\beta}}{d\tau^2}\\ +\Gamma^{\mu}_{\alpha\beta}\frac{dA^{\alpha}}{d\tau}\frac{dx^{\beta}}{d\tau}+\Gamma^{\mu}_{\alpha\beta}\Gamma^{\alpha}_{k\lambda}A^{k}\frac{dx^{\lambda}}{d\tau}\frac{dx^{\beta}}{d\tau}.\end{aligned} \tag{3.3.6}$$

Equation (3.3.6) reduced to

$$\begin{aligned}\frac{D^2A^{\mu}}{D\tau^2}=\frac{d^2A^{\mu}}{d\tau^2}+\Gamma^{\mu}_{\alpha\beta,\nu}\frac{dx^{\nu}}{d\tau}A^{\alpha}\frac{dx^{\beta}}{d\tau}+2\Gamma^{\mu}_{\alpha\beta}\frac{dA^{\alpha}}{d\tau}\frac{dx^{\beta}}{d\tau}\\ +\Gamma^{\mu}_{\alpha\beta}A^{\alpha}\frac{d^2x^{\beta}}{d\tau^2}+\Gamma^{\mu}_{\alpha\beta}\Gamma^{\alpha}_{k\lambda}A^{k}\frac{dx^{\lambda}}{d\tau}\frac{dx^{\beta}}{d\tau}.\end{aligned} \tag{3.3.7}$$

But, from geodesic equation, we have

$$\frac{d^2x^{\beta}}{d\tau^2}+\Gamma^{\beta}_{k\lambda}\frac{dx^{k}}{d\tau}\frac{dx^{\lambda}}{d\tau}=0. \tag{3.3.8}$$

Hence,

$$\frac{d^2x^{\beta}}{d\tau^2}=-\Gamma^{\beta}_{k\lambda}\frac{dx^{k}}{d\tau}\frac{dx^{\lambda}}{d\tau}. \tag{3.3.9}$$

Substituting equation (3.3.9) into equation (3.3.7), we get

$$\begin{aligned}\frac{D^2A^{\mu}}{D\tau^2}=\frac{d^2A^{\mu}}{d\tau^2}+\Gamma^{\mu}_{\alpha\beta,\nu}\frac{dx^{\nu}}{d\tau}A^{\alpha}\frac{dx^{\beta}}{d\tau}+2\Gamma^{\mu}_{\alpha\beta}\frac{dA^{\alpha}}{d\tau}\frac{dx^{\beta}}{d\tau}\\ -\Gamma^{\mu}_{\alpha\beta}\Gamma^{\beta}_{k\lambda}A^{\alpha}\frac{dx^{k}}{d\tau}\frac{dx^{\lambda}}{d\tau}+\Gamma^{\mu}_{\alpha\beta}\Gamma^{\alpha}_{k\lambda}A^{k}\frac{dx^{\lambda}}{d\tau}\frac{dx^{\beta}}{d\tau}.\end{aligned} \tag{3.3.10}$$

This is the second derivative of a vector A^{μ} along a geodesic curve. Now we can begin to calculate the relative acceleration of two particles moving on neighboring geodesics by writing down the equation of motion of each particles. If for a given value of τ(the same τ for both), the coordinates of the particles are $\chi^{\mu}(\tau)$ and $\chi^{\mu}(\tau)+\xi^{\mu}(\tau)$ then,

$$\frac{d^2x^{\mu}}{d\tau^2}+\Gamma^{\mu}_{\alpha\beta}(\chi)\frac{dx^{\alpha}}{d\tau}\frac{dx^{\beta}}{d\tau}=0, \tag{3.3.11}$$

is the equation of motion for the first particle and the following is the equation of motion for the second particle.

$$\frac{d^2}{d\tau^2}(\chi^{\mu}+\xi^{\mu})+\Gamma^{\mu}_{\alpha\beta}(\chi+\xi)\left(\frac{dx^{\alpha}}{d\tau}+\frac{d\xi^{\alpha}}{d\tau}\right)\left(\frac{dx^{\beta}}{d\tau}+\frac{d\xi^{\beta}}{d\tau}\right)=0. \tag{3.3.12}$$

By considering that ξ^μ and $\frac{d}{d\tau}\xi^\mu$ are infinitesimal i.e., the particles are near to each other and remain near each other for a fairly long time; let approximate the term $\Gamma^\mu_{\alpha\beta}(\chi+\xi)$ as following:

$$\Gamma^\mu_{\alpha\beta}(\chi+\xi) \approx \Gamma^\mu_{\alpha\beta}(\chi) + \Gamma^\mu_{\alpha\beta,\delta}\xi^\delta. \tag{3.3.13}$$

And keeping only the first terms in ξ, let calculate the difference between equation (3.3.11) and (3.3.12).

$$\frac{d^2x^\mu}{d\tau^2} + \Gamma^\mu_{\alpha\beta}(\chi)\frac{dx^\alpha}{d\tau}\frac{dx^\beta}{d\tau} = \frac{d^2}{d\tau^2}(\chi^\mu+\xi^\mu) + \Gamma^\mu_{\alpha\beta}(\chi+\xi) \left(\frac{dx^\alpha}{d\tau}+\frac{d\xi^\alpha}{d\tau}\right)\left(\frac{dx^\beta}{d\tau}+\frac{d\xi^\beta}{d\tau}\right). \tag{3.3.14}$$

By collecting on one side, we obtain

$$\frac{d^\mu}{d\tau^2}x^\mu + \Gamma^\mu_{\alpha\beta}(\chi)\frac{dx^\alpha}{d\tau}\frac{dx^\beta}{d\tau} - \frac{d^2}{d\tau^2}x^\mu - \frac{d^2}{d\tau^2}\xi^\mu - \Gamma^\mu_{\alpha\beta}(\chi)\left(\frac{dx^\alpha}{d\tau}+\frac{d\xi^\alpha}{d\tau}\right) \left(\frac{dx^\beta}{d\tau}+\frac{d\xi^\beta}{d\tau}\right) - \Gamma^\mu_{\alpha\beta}(\xi)\left(\frac{dx^\alpha}{d\tau}+\frac{d\xi^\alpha}{d\tau}\right)\left(\frac{dx^\beta}{d\tau}+\frac{d\xi^\beta}{d\tau}\right) = 0. \tag{3.3.15}$$

Canceling like terms in equation (3.3.15) results

$$\Gamma^\mu_{\alpha\beta}(\chi)\frac{dx^\alpha}{d\tau}\frac{dx^\beta}{d\tau} - \frac{d^2}{d\tau^2}\xi^\mu - (\Gamma^\mu_{\alpha\beta}(\chi)\frac{dx^\alpha}{d\tau} + \Gamma^\mu_{\alpha\beta}(\chi)\frac{d\xi^\alpha}{d\tau}) \left(\frac{dx^\beta}{d\tau}+\frac{d\xi^\beta}{d\tau}\right) - (\Gamma^\mu_{\alpha\beta}(\xi)\frac{dx^\alpha}{d\tau} + \Gamma^\mu_{\alpha\beta}(\xi)\frac{d\xi^\alpha}{d\tau})\left(\frac{dx^\beta}{d\tau}+\frac{d\xi^\beta}{d\tau}\right) = 0. \tag{3.3.16}$$

Expanding equation (3.3.16) gives

$$\Gamma^\mu_{\alpha\beta}(\chi)\frac{dx^\alpha}{d\tau}\frac{dx^\beta}{d\tau} - \frac{d^2}{d\tau^2}\xi^\mu - \Gamma^\mu_{\alpha\beta}(\chi)\frac{dx^\alpha}{d\tau}\frac{dx^\beta}{d\tau} - \Gamma^\mu_{\alpha\beta}(\chi)\frac{dx^\alpha}{d\tau}\frac{dx^\beta}{d\tau} - \Gamma^\mu_{\alpha\beta}(\chi)\frac{d\xi^\alpha}{d\tau}\frac{dx^\beta}{d\tau} - \Gamma^\mu_{\alpha\beta}(\chi)\frac{d\xi^\alpha}{d\tau}\frac{d\xi^\beta}{d\tau} - \Gamma^\mu_{\alpha\beta}(\xi)\frac{dx^\alpha}{d\tau}\frac{dx^\beta}{d\tau} - \Gamma^\mu_{\alpha\beta}(\xi)\frac{dx^\alpha}{d\tau}\frac{d\xi^\beta}{d\tau} - \Gamma^\mu_{\alpha\beta}(\xi)\frac{d\xi^\alpha}{d\tau}\frac{dx^\beta}{d\tau} - \Gamma^\mu_{\alpha\beta}(\xi)\frac{d\xi^\alpha}{d\tau}\frac{dx^\beta}{d\tau} = 0. \tag{3.3.17}$$

Equation (3.3.17) reduced to

$$-\frac{d^2}{d\tau^2}\xi^\mu - 2\Gamma^\mu_{\alpha\beta}(\chi)\frac{dx^\alpha}{d\tau}\frac{d\xi^\beta}{d\tau} - \Gamma^\mu_{\alpha\beta}(\chi)\frac{d\xi^\alpha}{d\tau}\frac{dx^\beta}{d\tau} - \Gamma^\mu_{\alpha\beta}(\xi)\left(\frac{dx^\alpha}{d\tau}+\frac{d\xi^\alpha}{d\tau}\right)\left(\frac{dx^\beta}{d\tau}+\frac{d\xi^\beta}{d\tau}\right) = 0. \tag{3.3.18}$$

Finally, we get

$$\frac{d^2}{d\tau^2}\xi^\mu = -\Gamma^\mu_{\alpha\beta,\delta}\xi^\delta \frac{dx^\alpha}{d\tau}\frac{dx^\beta}{d\tau} - 2\Gamma^\mu_{\alpha\beta}\frac{d\xi^\alpha}{d\tau}\frac{dx^\beta}{d\tau} \tag{3.3.19}$$

Now consider equation (3.3.10) to derive the second derivative of ξ^μ along the geodesic curve by substituting ξ^μ in place of A^μ.

$$\begin{aligned}\frac{D^2}{D\tau^2}\xi^\mu = \frac{d^2}{d\tau^2}\xi^\mu + \Gamma^\mu_{\alpha\beta,\nu}\xi^\alpha \frac{dx^\nu}{d\tau}\frac{dx^\beta}{d\tau} + 2\Gamma^\mu_{\alpha\beta}\frac{d\xi^\alpha}{d\tau}\frac{dx^\beta}{d\tau} \\ -\Gamma^\mu_{\alpha\beta}\Gamma^\beta_{k\lambda}\xi^\alpha \frac{dx^k}{d\tau}\frac{dx^\lambda}{d\tau} + \Gamma^\mu_{\alpha\beta}\Gamma^\alpha_{k\lambda}\xi^k \frac{dx^\lambda}{d\tau}\frac{dx^\beta}{d\tau}\end{aligned} \tag{3.3.20}$$

But, we derived the term $\frac{d^2}{d\tau^2}\xi^\mu$ in equation (3.3.19) and substitute it into (3.3.20).

$$\begin{aligned}\frac{D^2}{D\tau^2}\xi^\mu = -\Gamma^\mu_{\alpha\beta,\delta}\xi^\delta \frac{dx^\alpha}{d\tau}\frac{dx^\beta}{d\tau} - 2\Gamma^\mu_{\alpha\beta}\frac{d\xi^\alpha}{d\tau}\frac{dx^\beta}{d\tau} + \Gamma^\mu_{\alpha\beta,\nu}\xi^\alpha \frac{dx^\nu}{d\tau}\frac{dx^\beta}{d\tau} \\ +2\Gamma^\mu_{\alpha\beta}\frac{d\xi^\alpha}{d\tau}\frac{dx^\beta}{d\tau} - \Gamma^\mu_{\alpha\beta}\Gamma^\beta_{k\lambda}\xi^\alpha \frac{dx^k}{d\tau}\frac{dx^\lambda}{d\tau} + \Gamma^\mu_{\alpha\beta}\Gamma^\alpha_{k\lambda}\xi^k \frac{dx^\lambda}{d\tau}\frac{dx^\beta}{d\tau}.\end{aligned} \tag{3.3.21}$$

Canceling the second and the fourth terms in equation (3.3.21) and multiplying both sides by minus gives

$$\begin{aligned}-\frac{D^2}{D\tau^2}\xi^\mu = \Gamma^\mu_{\alpha\beta,\delta}\xi^\delta \frac{dx^\alpha}{d\tau}\frac{dx^\beta}{d\tau} - \Gamma^\mu_{\alpha\beta,\nu}\xi^\alpha \frac{dx^\nu}{d\tau}\frac{dx^\beta}{d\tau} \\ +\Gamma^\mu_{\alpha\beta}\Gamma^\beta_{k\lambda}\xi^\alpha \frac{dx^k}{d\tau}\frac{dx^\lambda}{d\tau} - \Gamma^\mu_{\alpha\beta}\Gamma^\alpha_{k\lambda}\xi^k \frac{dx^\lambda}{d\tau}\frac{dx^\beta}{d\tau}.\end{aligned} \tag{3.3.22}$$

Rearranging the indices in equation (3.3.22) results

$$\frac{D^2}{D\tau^2}\xi^\mu = -\frac{dx^\alpha}{d\tau}\frac{dx^\beta}{d\tau}\xi^\delta\{\Gamma^\mu_{\alpha\delta,\beta} - \Gamma^\mu_{\alpha\beta,\delta} + \Gamma^\epsilon_{\alpha\delta}\Gamma^\mu_{\beta\epsilon} - \Gamma^\epsilon_{\alpha\beta}\Gamma^\mu_{\delta\epsilon}\}. \tag{3.3.23}$$

But, the term in the bracket in equation (3.3.23) is equal to the Riemann-Christoffel curvature tensor, $R^\mu_{\alpha\delta\beta}$.

$$R^\mu_{\alpha\delta\beta} = \Gamma^\mu_{\alpha\delta,\beta} - \Gamma^\mu_{\alpha\beta,\delta} + \Gamma^\epsilon_{\alpha\delta}\Gamma^\mu_{\beta\epsilon} - \Gamma^\epsilon_{\alpha\beta}\Gamma^\mu_{\delta\epsilon}. \tag{3.3.24}$$

Substituting equation (3.3.24) into (3.3.23) gives,

$$\frac{D^2}{D\tau^2}\xi^\mu = -R^\mu_{\alpha\delta\beta}\xi^\delta \frac{dx^\alpha}{d\tau}\frac{dx^\beta}{d\tau}. \tag{3.3.25}$$

This is the equation of geodesic deviation, which gives the relativistic generalization of our Newtonian result for the tidal force. If space-time is flat then

$$R^{\mu}_{\alpha\delta\beta} = 0, \tag{3.3.26}$$

i.e., all components of the Riemann-Christoffel tensor are identically zero. This implies that the acceleration of the geodesic deviation is identically zero. However, if the space-time is curved then the geodesic separation changes along the world-line of neighboring particles.

For a comparison of the relativistic and Newtonian equation for the tidal force, assume that the particles under consideration are moving slowly with

$$\frac{dx^{\alpha}}{d\tau} \simeq (1,0,0,0) \qquad \text{and} \qquad \xi^0 = 0, \tag{3.3.27}$$

i.e., the particles' acceleration are compared at equal times and then equation (3.3.25) reduce to

$$\frac{d^2}{d\tau^2}\xi^k = -R^k_{0l0}\xi^l. \tag{3.3.28}$$

Hence, the tidal force can be written as

$$F^k_t = -mR^k_{0l0}\xi^l, \tag{3.3.29}$$

where m is the mass of the particle and ξ^l its displacement from the origin. This equation is valid only if the displacement and the velocity are small. To agree this equation with that of the Newtonian expression in equation (3.2.15), we have to make a linear approximation by omitting the two terms in $\Gamma^{\alpha}_{\beta\mu}$ in equation (3.3.24). This approximation becomes

$$\Gamma^{\alpha}_{\beta\mu} = \frac{k}{2}\eta^{\alpha\delta}(h_{\delta\beta,\mu} + h_{\mu\delta,\beta} - h_{\beta\mu,\delta}). \tag{3.3.30}$$

Substituting equation (3.3.30) into (3.3.24) and rearranging indices results

$$R^{\mu}_{\beta\mu\nu} \simeq -\frac{k}{2}\eta^{\alpha\delta}(h_{\mu\delta,\beta,\nu} - h_{\beta\mu,\delta,\nu} - h_{\nu\delta,\beta,\mu} + h_{\beta\nu,\delta,\mu}). \tag{3.3.31}$$

From equation (3.3.31), R^k_{0l0} can be written as

$$R^k_{0l0} \simeq -\frac{k}{2}(h_{lk,0,0} - h_{0l,k,0} - h_{0k,0,l} + h_{00,k,l}). \tag{3.3.32}$$

In the Newtonian limit all the terms containing time derivative can be omitted and in the absence of matter ($T_{\mu\nu} = 0$), the equation for statical Newtonian potential is given by

$$\Phi = \frac{1}{2}kh_{00}. \tag{3.3.33}$$

Using equation (3.3.33), we find

$$R^k_{0l0} = \frac{\partial^2\Phi}{\partial x^k \partial x^l}, \tag{3.3.34}$$

which is the same result with equation (3.2.5). The tidal force we obtained in equation (3.3.29) satisfy

$$\frac{\partial F^k_t}{\partial \xi^k} = 0, \tag{3.3.35}$$

this means, the tidal force field can be represented graphically by field line .

$$\begin{aligned}
\frac{\partial F^k_t}{\partial \xi^k} &= \frac{\partial}{\partial \xi^k}(-mR^k_{0l0}\xi^l) \\
\frac{\partial F^k_t}{\partial \xi^k} &= -\frac{\partial}{\partial \xi^k}\left(m\frac{\partial^2\Phi}{\partial x^k \partial x^l}\xi^l\right) \\
\frac{\partial F^k_t}{\partial \xi^k} &= -m\frac{\partial \xi^l}{\partial \xi^k}\frac{\partial^2\Phi}{\partial x^k \partial x^l} \\
\frac{\partial F^k_t}{\partial \xi^k} &= -m\delta^l_k\frac{\partial^2\Phi}{\partial x^k \partial x^l} \\
\frac{\partial F^k_t}{\partial \xi^k} &= -m\delta^l_l\frac{\partial^2\Phi}{\partial x^k \partial x^k} \\
\frac{\partial F^k_t}{\partial \xi^k} &= 0,
\end{aligned} \tag{3.3.36}$$

where

$$\delta^l_l = 1 \qquad \text{and} \qquad \frac{\partial^2\Phi}{\partial x^k \partial x^k} = 0, \tag{3.3.37}$$

because Φ is a constant.

3.4 Time for Gravitational Tidal Locking

We consider two point masses, m_{co} at point B(mass of the core) and m_{cr} at point A (mass of the crust) of neutron star executing circular orbits about their common center mass with angular velocity of crust Ω_{cr} as in fig.(3.1), to calculate the centrifugal and gravitational potential at some point D in the vicinity of point B. It is convenient to adopt spherical coordinates centered at the point B. We assume that the mass distribution of m_{co} is around the center of mass C, but it is not rotating about an axis passing through its center of mass. Each constituent point of m_{co} executes circular motion of angular velocity Ω_{cr} and radius b (the distance between the center of mass and the core of neutron star).

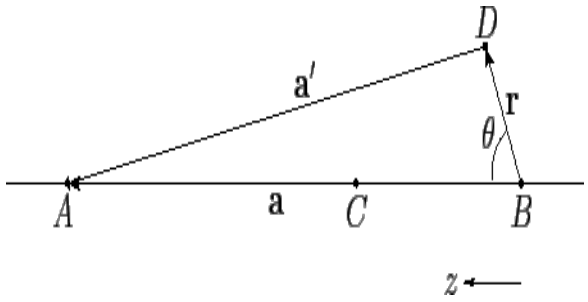

Figure 3.1: Used for calculation of tidal potential.

Hence, each point experiences the same centrifugal acceleration, which is given by

$$\mathbf{a}_c = -\Omega_{cr}^2 b\hat{z} = -\nabla\phi_c, \tag{3.4.1}$$

where Φ_c is the centrifugal potential and written as

$$\Phi_c = \Omega_{cr}^2 brcos\theta. \tag{3.4.2}$$

Here r is the distance between the point D and the core of neutron star and θ is an angle of rotation. But, from Kepler's 3^{rd} law we can write the term Ω_{cr}^2 as following.

$$\Omega_{cr}^2 a^3 = G(m_{co} + m_{cr})$$

$$\Omega_{cr}^2 = \frac{G}{a^3}(m_{co} + m_{cr}), \tag{3.4.3}$$

and the term b as

$$b = a\left(\frac{m_{cr}}{m_{co} + m_{cr}}\right). \tag{3.4.4}$$

Here G is gravitational constant and a is the distance between the core and the crust of neutron star. By substituting equation (3.4.3) and (3.4.4) into (3.4.2), we get

$$\Phi_c = \frac{Gm_{cr}a}{a^3}\left(\frac{m_{co} + m_{cr}}{m_{co} + m_{cr}}\right) rcos\theta$$

$$\Phi_c = \frac{Gm_{cr}}{a^2} rcos\theta = \frac{Gm_{cr}}{a}\frac{r}{a}cos\theta$$

$$\Phi_c = \frac{Gm_{cr}}{a}\left[1 + \frac{r}{a}p_1(cos\theta)\right], \tag{3.4.5}$$

which has a Legendre polynomial from.

The gravitational acceleration at point D due to the mass m_{cr} is given by

$$\mathbf{a}_g = -\nabla\Phi_g. \tag{3.4.6}$$

Where Φ_g is gravitational potential and it is given by

$$\Phi_g = -\frac{Gm_{cr}}{a'}, \tag{3.4.7}$$

where a' is the distance between the point D and the crust of the neutron star and let derive it using cosine law.

$$\mathbf{a}'.\mathbf{a}' = \mathbf{a}.\mathbf{a} + \mathbf{r}.\mathbf{r} - 2\mathbf{a}.\mathbf{r}$$

$$a'^2 = a^2 + r^2 - 2arcos\theta$$

$$a' = (a^2 + r^2 - 2arcos\theta)^{\frac{1}{2}}. \tag{3.4.8}$$

By taking the inverse of equation (3.4.8) and expanding it , we obtain

$$a'^{-1} = (a^2 + r^2 - 2arcos\theta)^{-\frac{1}{2}}$$

$$a'^{-1} = a^{-1}\sum_{n=0}^{\infty}\left(\frac{r}{a}\right)^n P_n(cos\theta), \tag{3.4.9}$$

where P_n is Legendre polynomial. Substituting equation (3.4.9) into (3.4.7) gives

$$\Phi_g = -\frac{Gm_{cr}}{a'} = -Gm_{cr}a'^{-1}$$

$$\Phi_g = -Gm_{cr}a^{-1}\sum_{n=0}^{\infty}\left(\frac{r}{a}\right)^n P_n(cos\theta)$$

$$\Phi_g = -\frac{Gm_{cr}}{a}\sum_{n=0}^{\infty}\left(\frac{r}{a}\right)^n P_n(cos\theta). \tag{3.4.10}$$

By expanding equation (3.4.10) to the second order in $\frac{r}{a}$ gives

$$\Phi_g \simeq -\frac{Gm_{cr}}{a}\left[1 + \frac{r}{a}p_1(cos\theta) + \frac{r^2}{a^2}P_2(cos\theta) + ...\right]. \tag{3.4.11}$$

Now, we can calculate the tidal potential using equation (3.4.5) and (3.4.11) as

$$\Phi_t \simeq \frac{Gm_{cr}}{a}\left[1 + \frac{r}{a}p_1(cos\theta)\right] -$$

$$\frac{Gm_{cr}}{a}\left[1+\frac{r}{a}p_1(cos\theta)+\frac{r^2}{a^2}P_2(cos\theta)\right]$$

$$\Phi_t \simeq \frac{Gm_{cr}}{a}+\frac{Gm_{cr}}{a}\frac{r}{a}p_1(cos\theta)-\frac{Gm_{cr}}{a}$$

$$-\frac{Gm_{cr}}{a}\frac{r}{a}p_1(cos\theta)-\frac{Gm_{cr}}{a}\frac{r^2}{a^2}P_2(cos\theta)$$

$$\Phi_t \simeq -\frac{Gm_{cr}}{a}\frac{r^2}{a^2}P_2(cos\theta). \tag{3.4.12}$$

By considering the spherical coordinate, the total external gravitational potential is given as

$$\Phi = -\frac{Gm_{co}}{r}-Gm_{co}\xi\frac{R^2}{r^3}P_2(cos\theta),$$

where $\xi = \frac{m_{cr}}{m_{co}+m_{cr}}(\frac{R}{r})^3$ is a dimensionless parameter , but m_{cr} is very small as compared with m_{co} and we can write as $m_{co}+m_{cr}\simeq m_{co}$,

$$\Phi = -\frac{Gm_{co}}{r}-Gm_{co}\frac{R^2}{r^3}\left[\frac{m_{cr}}{m_{co}}\left(\frac{R}{a}\right)^3\right]\frac{1}{2}(3cos^2\theta-1)$$

$$\Phi = -\frac{Gm_{co}}{r}-\frac{1}{2}Gm_{cr}\frac{R^2}{r^3}\left(\frac{R}{a}\right)^3(3cos^2\theta-1). \tag{3.4.13}$$

The tidal torque about the center of the core, that gravitational field exerts on the crust is given as

$$\tau_t = -m_{cr}\frac{\partial\Phi}{\partial\theta}|_{r=a}$$

$$\tau_t = -m_{cr}\frac{\partial}{\partial\theta}\left[-\frac{Gm_{co}}{r}-\frac{1}{2}Gm_{cr}\frac{R^2}{r^3}\left(\frac{R}{a}\right)^3(3cos^2\theta-1)\right]$$

$$\tau_t = -m_{cr}\left[-\frac{1}{2}Gm_{cr}\frac{R^2}{r^3}\left(\frac{R}{a}\right)^3\frac{\partial}{\partial\theta}(3cos^2\theta-1)\right]$$

$$\tau_t = -m_{cr}\left[-\frac{3}{2}Gm_{cr}\frac{R^2}{r^3}\left(\frac{R}{a}\right)^3(-2cos\theta sin\theta)\right]$$

$$\tau_t = -\frac{3}{2}Gm_{cr}^2\frac{R^2}{r^3}\left(\frac{R}{a}\right)^3 sin2\theta|_{r=a}$$

$$\tau_t \simeq -\frac{3}{2}\frac{Gm_{cr}^2}{R}\left(\frac{R}{a}\right)^6 sin2\theta. \tag{3.4.14}$$

The tidal torque due the rotation of the core is equal with that of the tidal torque exerted on the crust due to gravitational field, but opposite in direction and given as

$$\tau_t = I\alpha = \frac{2}{5}MR^2\dot{\mathbf{\Omega}}_{co} = \frac{2}{5}(m_{co}+m_{cr})R^2\dot{\mathbf{\Omega}}_{co}. \tag{3.4.15}$$

By equating equation (3.4.14) and (3.4.15), we obtain

$$\dot{\mathbf{\Omega}}_{co} = -\frac{15}{4}\frac{G}{R^3}\left(\frac{m_{cr}^2}{m_{co}+m_{cr}}\right)\left(\frac{R}{a}\right)^6 sin2\theta$$

$$\dot{\mathbf{\Omega}}_{co} = -\frac{15}{4}\frac{G}{a^3}\left(\frac{m_{cr}^2}{m_{co}+m_{cr}}\right)\left(\frac{R}{a}\right)^3 sin2\theta$$

$$\dot{\mathbf{\Omega}}_{co} = -\frac{15}{4}\frac{G}{a^3}(m_{co}+m_{cr})\left(\frac{m_{cr}}{m_{co}+m_{cr}}\right)^2\left(\frac{R}{a}\right)^3 sin2\theta$$

$$\dot{\mathbf{\Omega}}_{co} = -\frac{15}{4}\Omega_{cr}^2\left(\frac{m_{cr}}{m_{co}+m_{cr}}\right)^2\left(\frac{R}{a}\right)^3 sin2\theta,$$

where $\Omega_{cr}^2 = \frac{G}{a^3}(m_{co}+m_{cr})$ and $m_{co}+m_{cr} \simeq m_{co}$.

$$\dot{\mathbf{\Omega}}_{co} = -\frac{15}{4}\Omega_{cr}^2\left(\frac{m_{cr}}{m_{co}}\right)^2\left(\frac{R}{a}\right)^3 sin2\theta. \tag{3.4.16}$$

This an angular acceleration and the minus sign shows the retardation of angular acceleration. To obtain the angular frequency, we divided both sides of equation (3.4.16) by $\mathbf{\Omega}_{co}$.

$$\frac{\dot{\mathbf{\Omega}}_{co}}{\mathbf{\Omega}_{co}} = -\frac{15}{4}\left(\frac{\mathbf{\Omega}_{cr}^2}{\mathbf{\Omega}_{co}}\right)\left(\frac{m_{cr}}{m_{co}}\right)^2\left(\frac{R}{a}\right)^3 sin2\theta. \tag{3.4.17}$$

The timescale for the tidal torque to reduce significantly, the rotational angular velocity of the core is given as

$$T \simeq \frac{\mathbf{\Omega}_{co}}{|\dot{\mathbf{\Omega}}_{co}|}$$

$$T \simeq \frac{4\mathbf{\Omega}_{co}}{15\mathbf{\Omega}_{cr}^2}\left(\frac{m_{cr}}{m_{co}}\right)^2\left(\frac{a}{R}\right)^3\frac{1}{sin2\theta}. \tag{3.4.18}$$

As observation shows, an angle θ is very small, so for very small angle θ, $sin\theta$ can be written as $sin\theta \simeq \theta$. Hence, equation (3.4.18) becomes

$$T \simeq \frac{4\mathbf{\Omega}_{co}}{15\mathbf{\Omega}_{cr}^2}\left(\frac{m_{cr}}{m_{co}}\right)^2\left(\frac{a}{R}\right)^3\frac{1}{2\theta}$$

$$T_{syc} \simeq \frac{2\mathbf{\Omega}_{co}k}{15\mathbf{\Omega}_{cr}^{2}\theta}\left(\frac{a}{R}\right)^{3}, \tag{3.4.19}$$

where

$$k = \left(\frac{m_{cr}}{m_{co}}\right)^{2}. \tag{3.4.20}$$

Here a is the distance between the core and the crust of the neutron star (or radius of the crust) and R is the radius of the core of the neutron star. The equation we obtained in (3.4.19) is the equation that used to calculate the time-scale at which the crust and the core of neutron star to be tidally locked. This time is called synchronous time and at this time there is no phase lag, because tidal torque will be zero.

Chapter 4

Result and Discussion

From all pulsars, PSR B1821-24 has a typically small glitch amplitude, with the smallest glitch of amount $\frac{\Delta\Omega}{\Omega} = 8 \times 10^{-12}$ [52], while PSR J164710.2-455216 has the largest glitch amount of $\frac{\Delta\Omega}{\Omega} = 6 \times 10^{-5}$ [53]. The time-scale for the spin up is currently unresolved by observations, although it is constrained to less than ~ 30 s in the Vela pulsar [54], while the recovery lasts from days to weeks.

In 102 pulsars 315 glitch events have been observed [1, 2]. Some pulsars have experienced glitches many times, some only once, and others never. Of the 102 known glitching pulsars, 54 have glitched only once, while 6 have glitched more than 10 times [1, 2]. Five pulsars have glitched more than ten times: the Crab 27 times [55], PSR J1740-3015 23 times [56], PSR J0537-6910 20 times [57], Vela 17 times [54] and PSR J1341-6220 12 times [58].

Figure 4.1 presents the glitch rate ($\dot{N}_g$, number of glitches per year) versus characteristic age τ_c.

The glitch rate is determined by dividing the number of observed glitches by the total observation time for all pulsars that have glitched at least once, and have been observed for at least three years. The most frequent glitchers are labelled on the plot. The plot demonstrates a decrease in glitch activity with increasing characteristic age, supporting the findings of previous studies [59, 60].

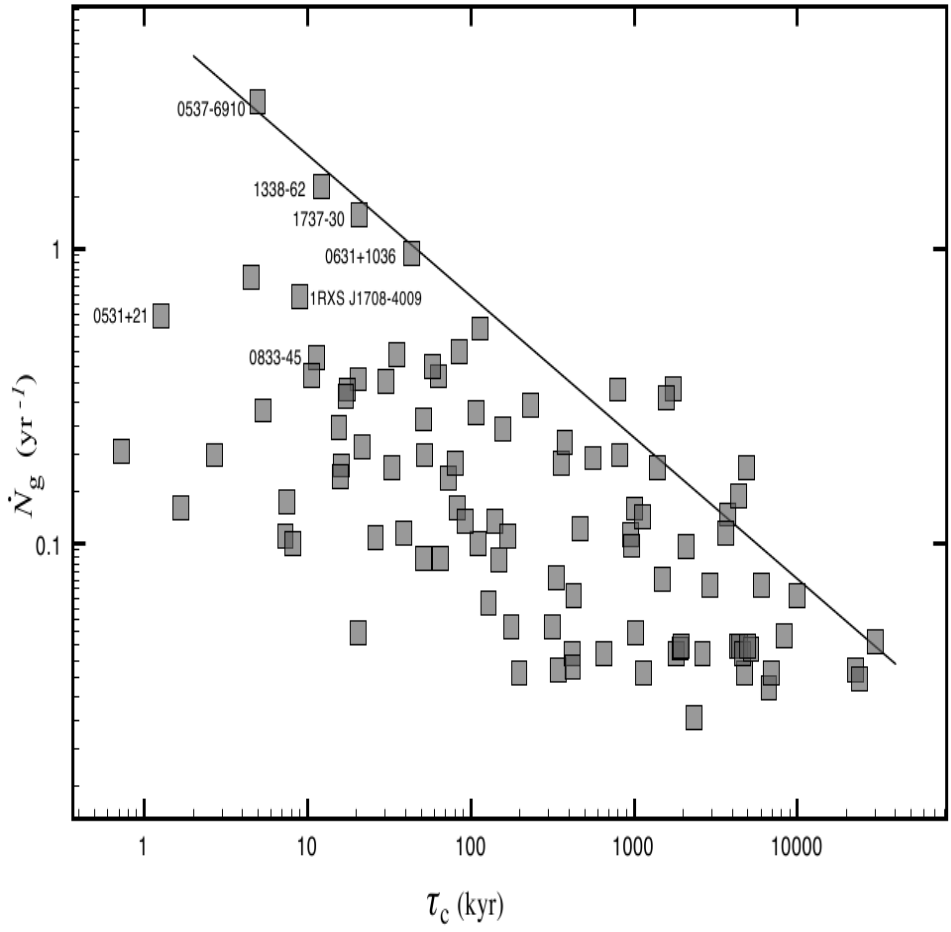

Figure 4.1: Number of glitches per year $\dot{N}_g$ for individual pulsars versus the characteristic age for all pulsars observed for at least 3 years and with one or more glitch detected. The straight line is a linear fit to the maximum value of $\dot{N}_g$ in each half decade of characteristic age. Taken from Espinoza et al. (2011).

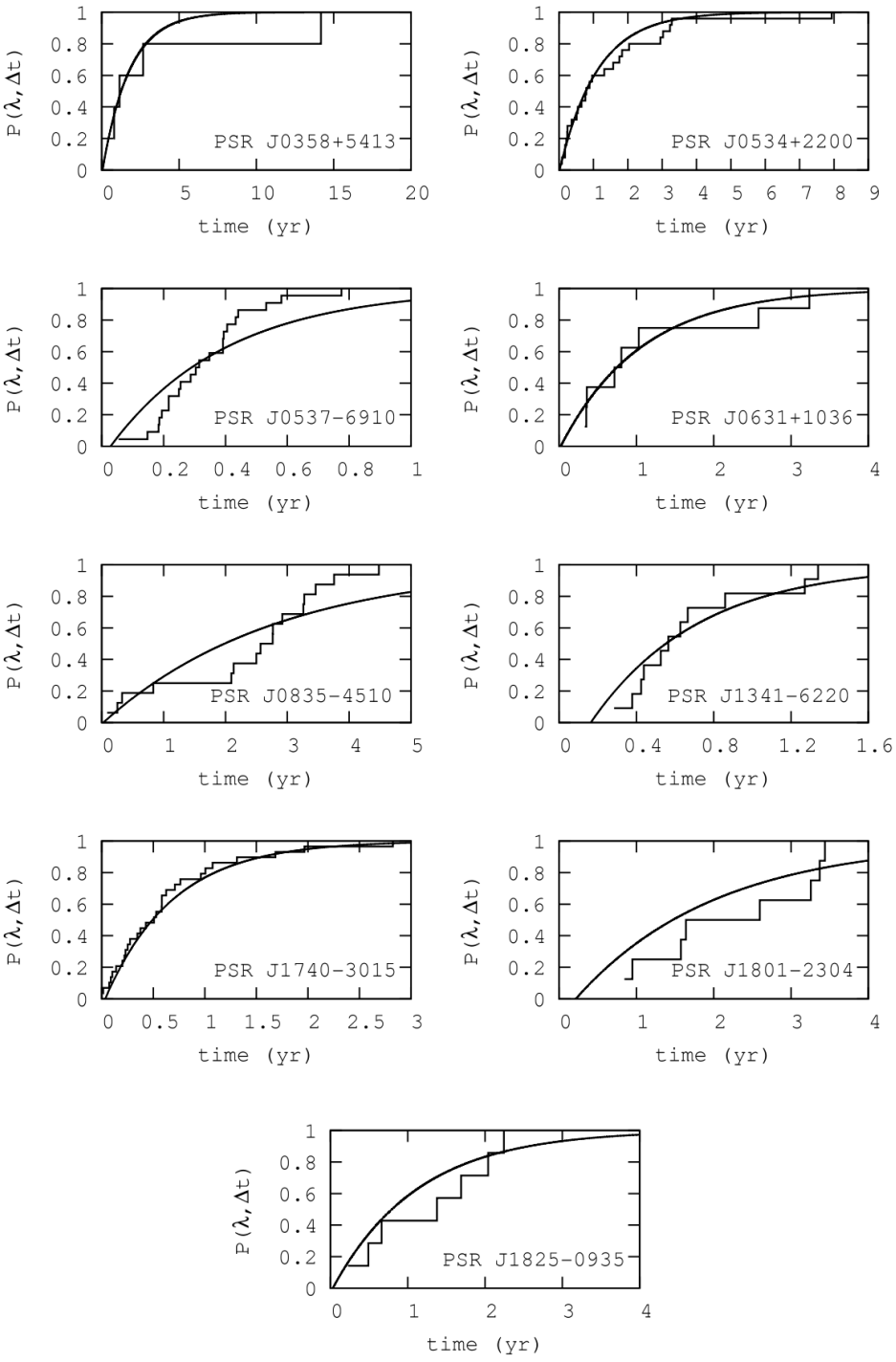

Figure 4.2: Cumulative distribution of glitch waiting times $\triangle t$ (measured in yr) for the nine pulsars that have glitched more than five times. The observational data (histograms) are plotted together with the best Poisson fits (solid curves).Taken from Melatos et al. (2008).

Glitch activity peaks for pulsars with characteristic age $\tau_c \sim 10kyr$ and decreases for larger τ_c, disappearing for objects with $\tau_c > 20Myr$ [2]. However, there are exceptions, such as PSR B1509-58 (with $\tau_c \sim 1.5kyr$) which has not glitched once in over 21 years of observations [61]. The glitch activity is smaller in the very young pulsars ($\tau_c < 1kyr$). Figure 4.2 shows the plot of the waiting-time distribution versus characteristic age for nine most glitchers pulsars. The value of the mean glitching rate λ is between $0.35yr^{-1}$ and $2.6yr^{-1}$, because the study shows its value between these numbers.

As we see in figure 4.1, the number of glitches decreases as characteristic age of pulsars increase. There is something behind this to be happened. This is electromagnetic braking torque and gravitational tidal torque, which make the rigid crust cannot adjust to the new balance of centrifugal and gravitational forces, during the star spins down. These forces produce centrifugal and gravitational potential respectively. The produced potential cause for creation of tidal torque between the crust and the core of neutron stars. This tidal torque is the mean cause for the decreasing of a number of glitches with the increasing ages of the pulsars. As the pulsars get old in ages, the effect of this tidal torque will more increases and causes for the tidal locking of the crust and the core of the neutron stars.

From point view of their observational data, Espinoza et.al., suggested that if the ages of the pulsars are greater than 20Myr, the glitches activity will disappear [2]. This supports our model, because if the crust and the core of the neutron star tidally locked, the perturbation would not occur in the neutron star. This leads to the disappearance of the glitches activity.

We derived in equation (3.73), the time at which the crust and the core of the neutron star will be tidally locked and after this time there will no be glitches activity, because the tidal torque will be zero. This equation is,

$$T_{syc} \simeq \frac{2\mathbf{\Omega}_{co}k}{15\mathbf{\Omega}_{cr}^2\theta}\left(\frac{a}{R}\right)^3, \tag{4.0.1}$$

where

$$k = \left(\frac{m_{cr}}{m_{co}}\right)^2. \tag{4.0.2}$$

For instance, for the crab pulsar with the following data: $\Omega_{co} = 1001 rads^{-1}$, $\Omega_{cr} = 2001 rads^{-1}$, and $\theta = 10^{-14} rad$ [62]; $m_{co} = 1.2 M_{\odot}$, $m_{cr} = 1.23 \times 10^{-3} M_{\odot}$, $R = 9km$, and $a = 10km$ [17]; the time for gravitational tidal locking (synchronous time) will be

$$T_{syc} \simeq \frac{2\mathbf{\Omega}_{co} k}{15\mathbf{\Omega}_{cr}^2 \theta} \left(\frac{a}{R}\right)^3 \simeq 1.38 \times 10^8 yr. \tag{4.0.3}$$

After this time the crust and the core will have a comman angular velocity and the glitches activity will not occur.

Conclusion

In this thesis, we attempted to address the causes for the decrement of glitches with the increment of the ages of the pulsars.

- We derived an equation for tidal force and tidal torque, which govern rotation of neutron stars.

- Based on, the equation of tidal torque, we derived the time at which the crust and the core of neutron star will be tidally locked. After the crust and the core of neutron star tidally locked, the tidal torque will be zero. If the tidal torque is zero, then nothing can perturb the rotation of neutron star. Hence, spinning down and spinning up of angular frequency cannot occur. This results, the phase lag to be zero, which causes for the decrement of glitches, even for disappearance of glitches with the increment of pulsars' ages.

- Vortex pinning between the inner crust and the super-fluid component decreases as the pulsars get old in ages more and more. This may be one factor for the decrement of the glitches activity.

- The tidal interaction (tidal force and tidal torque) between the crust and the core of neutron star plays a great role for the decrement of the glitches at old ages of the pulsars.

Bibliography

[1] Melatos, A.; Peralta, C. and Wyithe, J. S. B. , Avalanche Dynamics of Radio Pulsar Glitches, The Astrophysical Journal, 672, 1103 (2008).

[2] Espinoza C. M. , Lye A. G. , Stappers B. W. , Kramer M. , Monthly Notes of the Royal Astronomical Society, 414, 1679 (2011).

[3] Anderson P. W. , Itoh N. , Nature, 256, 25 (1975).

[4] Alpar M. A. , The Astrophysical Journal, 213, 527 (1977).

[5] Pines D. , Shaham J. , Alpar M. A. , Anderson P. W. , Progress Theoretical Physics Supplement, 69, 376 (1980).

[6] Jayanta R. , Yashwant G. , and Wojciech L, Observations of four glitches in young pulsar J1833-1034 and study of its glitch activity. Royal Astronomical Society Journal, may (2012).

[7] W. Baade and F. Zwicky, Cosmic rays from supernovae. Proceedings of the National Academy of Sciences of the United States of America, 20: 259-263, May (1934).

[8] B. W. Carroll and D. A. Ostlie , An Introduction to Modern Astrophysics, Addison Wesley,(1996).

[9] S. L. Shapiro and S. A. Teukolsky: Black Holes, White Dwarfs, and Neutron Stars, The Physics of Compact Objects, Wiley-Interscience, (1983).

[10] J. M. Lattimer and M. Prakash. Neutron star observations: Prognosis for equation of state constraints. Physics Reports, 442: 109-165, April (2007).

[11] A. J. Faulkner, M. Kramer, A. G. Lyne, R. N. Manchester, M. A. McLaughlin, I. H. Stairs, G. Hobbs, A. Possenti, D. R. Lorimer, N. D'Amico, F. Camilo, and M. Burgay. PSR J1756-2251: A new relativistic double neutron star system. The Astrophysical Journal, 618: L119-L122, January (2005).

[12] J. R. Oppenheimer and G. M. Volkoff. On massive neutron cores. Physical Review, 55: 374-381, February (1939).

[13] R. C. Tolman. Static solutions of Einstein's field equations for spheres of fluid. Physical Review, 55: 364-373, February (1939).

[14] Miller, M. C. , Monthly Notes of the Royal Astronomical Society, 255, 129 (1992).

[15] Rajagopal, M. , Romani, R. W. , Miller, M. C. , Astrophysical Journal, 479, 347 (1997).

[16] E. H. Gudmundsson, C. J. Pethick, and R. I. Epstein, Structure of neutron star envelopes, American Astronomical Society Journal, Ferbruary (1983).

[17] Barbara Partricelli J. A. , Rueda H. , R. Ruffini: The crust of neutron stars. 3^{rd} Stueckelberg workshop on Relativistic field theories, July (2003).

[18] Lorenz, C. P. , Ravenhall, D. G. , and Pethick, C. J. , Physical Review Letters , 70, 379 (1993).

[19] Pethick, C. J. , Ravenhall, D. G. , Lorenz, C. P. , Nuclear Physics A, 584, 675 (1995).

[20] Heiselberg, H., Pandharipande, V. , Annual Review of Nuclear Particle Physics, 50, 481 (2000).

[21] Gold,T. , Nature, 218, 731 (1968).

[22] Hewish, A. , Bell, S. J. , Pilkington, J. D. H , Scott, P. F. , Collins, R. A. , Nature, 217, 709 (1968).

[23] Pilkington, J. D. H. , Hewish, A. , Bell, S. J. , Cole, T. W. , Nature, 218, 126 (1968).

[24] Hewish, A. , Speech delivered upon receiving the Nobel Prize in (1974).

[25] A. B. Migdal, Soviet Journal of Experimental and Theoretical Physics, 10, 176 (1960).

[26] D. G. Yakovlev and C. J. Pethick, Annual Review of Astronomy and Astrophysics (2004).

[27] Kapitza, P. L. , Dk. Akad. Nauk SSSR, 18, 21 (1938).

[28] Harling, O. K. , Physical Review Letters, 24, 1046, (1970).

[29] Landau, L. D. , Lifshitz, E. M. , Fluid Mechanics, 2nd Edition, Pergamon Press (1987).

[30] Troup, G. J. , Optical Coherence Theory Developments (1967).

[31] Andronikashvili, E. L. , Zh. Eksp. Theor. Fiz., 16, 780 (1946).

[32] Osborne, D. V. , Proc. Phys. Soc. , A63, 909 (1950).

[33] Vinen, W. F. , Nature, 181, 1524 (1958).

[34] Hall, H. E. , Vinen, W. F. , Proc. Roy. Soc. A, 238, 204, 215 (1956).

[35] Ginzburg, V. L. , Kirzhnits, D. A. , Zh. Eksp. Theor. Fiz. , 47 (2006).

[36] Lyne, A. G. and Graham-Smith, F. Pulsar astronomy, Cambridge University Press (1998).

[37] Lyne, A. G. , Shemar, S. L. , and Graham Smith, F. Monthly Notes of the Royal Astronomical Society, 315, 534 (2000).

[38] Negele, J. W. , and Vautherin, D. Nuclear Physics A, 207, 298 (1973).

[39] Sonin, E. B. Review of Modern Physics , 59, 87 (1987).

[40] Alpar M. A. , Anderson P. W. , Pines D. , Shaham J. , Astrophysics Journal, 276, 325 (1984).

[41] Anderson P. W. , Alpar M. A. , Pines D. , Shaham J. , Philos. Magazine A, 45, 227 (1982).

[42] Jones P. B. , Physical Review Letters, 79, 792 (1997).

[43] Grill F. , PhD thesis, University of Milan (2011).

[44] Pizzochero P. M. , Astrophysical Journal, 743, L20 (2011).

[45] Blandford, R. D. , Hewish, A. , Lyne, A. G. , Mestel, L. and Graham-Smith, F. , Pulsarsas Physics Laboratories, The Royal Society Oxford University Press, 1993.

[46] Alpar, M. A. , Chau, H. F. , Cheng, K. S. and Pines, D. , Postglitch relaxation of the Vela pulsar after its first eight large glitches - A reevaluation with the vortex creep model, The Astrophysical Journal 409, 345 (1993).

[47] Sedrakian, D. M. and Hairapetian, M. V. , Relaxation of the Angular Velocity of the Vela Pulsar Following Its First Eight Glitches, Astrophysics Journal, 44, 255 (2001).

[48] Alpar, M. A. , Langer, S. and Sauls, J. A. , Astrophysical Journal, 282, 533 (1984).

[49] Alpar, M. A. , Anderson, P. W. , Pines, D. and Shaham, J. , Astrophysical Journal, 276, 325 (1984a).

[50] Alpar, M. A. , Brinkmann, W. , Kiziloglu, U. , Ogelman, H. and Pines, D. , Astronomy and Astrophysics, 177, 101 (1987).

[51] Ohanian H. C. and Ruffini R. , Gravitation and Space-time, W. W. Norton and Company, Second Edition, 1994.

[52] Cognard, I. and Backer, D. C. , A Microglitch in the Millisecond Pulsar PSR B1821-24 in M28, The Astrophysical Journal 612, L125 (2004).

[53] Israel, G. L. , Campana, S. , Dall'Osso, S. , Muno, M. P. , Cummings, J. , Perna, R. and Stella, L. , The Post-Burst Awakening of the Anomalous X-Ray Pulsar in Westerlund 1, The Astrophysical Journal 664, 448 (2007).

[54] Dodson, R. , Lewis, D. and McCulloch, P. , Two decades of pulsar timing of vela, Astrophysics and Space Science 308, 585 (2007).

[55] Wong, T. , Backer, D. C. and Lyne, A. G. , Observations of a Series of Six Recent Glitches in the Crab Pulsar, The Astrophysical Journal 548, 447 (2001).

[56] Zou, W. Z. , Wang, N. , Manchester, R. N. , Urama, J. O. Hobbs, G. Liu, Z. Y. and Yuan, J. P. , Observations of six glitches in PSR B1737-30, Monthly Notices of the Royal Astronomical Society 384, 1063 (2008).

[57] Middleditch, J. , Marshall, F. E. , Wang, Q. D. , Gotthelf, E. V. and Zhang, W. , Predicting the Starquakes in PSR J0537-6910, The Astrophysical Journal 652, 1531 (2006).

[58] Wang, N. , Wu, X. , Manchester, R. N. , Zhang, J. , Lyne, A. G. and Yusup, A. , A Large Glitch in the Crab Pulsar, Chinese Journal of Astronomy and Astrophysics 1, 195 (2001).

[59] Urama, J. O. and Okeke, P. N. , Vela-size glitch rates in youthful pulsars, Monthly Notices of the Royal Astronomical Society 310, 313 (1999).

[60] Peralta, C. A. , Superfluid spherical Couette flow and rotational irregularities in pulsars, PhD thesis, University of Melbourne, Australia (2007).

[61] Livingstone, M. A. , Kaspi, V. M. , Gavriil, F. P. and Manchester, R. N. , 21 Years of Timing PSR B1509-58, The Astrophysical Journal 619, 1046 (2005b).

[62] arXiv:astro ph/9801070v1, 1998.

Declaration

This thesis is my original work, has not been presented for a degree in any other University and that all the sources of material used for the thesis have been dully acknowledged.

Name: Kuba Girma

Signature:– – – – – – – – – – – –

Place and time of submission: Addis Ababa University, June 2014

This thesis has been submitted for examination with my approval as University advisor.

Name: Dr. Legese Wetro

Signature:– – – – – – – – – ––